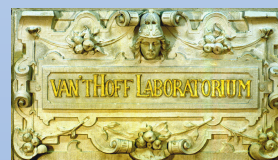# Diffusion of Flexible Colloidal Clusters

Nathalie Ligthart

Utrecht University

VAN 'T HOFF LABORATORIUM

Diffusion of Flexible Colloidal Clusters

Nathalie E.G. Ligthart

Abstract

Colloidal particles exhibit Brownian motion when suspended in a liquid and they are large enough to visualize with optical microscopy. These characteristics make colloidal systems suitable models for studying thermal motion. The diffusion of colloids of various shapes has been studied and Brownian motion of colloids has been found to be influenced by their shape. In this work, we investigated the influence of a constantly changing shape of the colloid on the colloid's Brownian motion. This can give insight in the diffusion of many flexible compounds in nature and industry, such as molecules, polymers, proteins and bacterial flagellae. We studied and compared the diffusion of rigid- and freely jointed trimers as well as hydrodynamic correlations between the trimers' time-dependent position, orientation and bond angle. We find two differences in the Brownian motion of rigid and freely jointed trimers. The first is that trimers with a changing internal angle have lower translational and rotational diffusion coefficients than their rigid counterparts. The second difference pertains to the hydrodynamic correlations in the diffusion tensor of the clusters. We find a negative correlation between diffusion along the short axis of the freely jointed trimers and their internal angle. This observation shows that the translation of these flexible particles is coupled to a conformational change of the cluster. Lastly, we show that flexible chains can be made with the same procedure. Analysis of those can give insight into diffusion of flexible structures like polymers and proteins.

Contents

Preface

In the Netherlands, every ray of sunshine is celebrated. When it is a sunny and sufficiently warm day, people in the cities flock outside to cruise along on little boats on the canal. In addition to their love of the sun and water, these people all have something else in common; they use hydrodynamic coupling to move over the water and enjoy their day.

The forward movements of these boats is caused by the turning of propellers in the water. If the propeller blades were straight sticks instead of curved blades like those shown in Figure 1a, their turning would not push the boat forward. It is due to a certain asymmetry in the shape of the propellers that makes it possible to induce a coupling of the rotational motion and a forward thrust.

Recently, this coupling between one type of motion and another has also been found to occur in microscopic objects with a size between 1 nm and 1 µm. A nice example of such an object is a boomerang colloidal particle, of which a trajectory is shown in Figure 1b. This trajectory clearly shows that each displacement of the colloid is paired with a rotation. This is surprising because colloidal objects in solution exhibit Brownian motion (random walks), not a steered motion like the continuous rotation of a propeller.

It is thus clear that the motion of microscopic objects is influenced by their shape, just like on the macroscopic scale. But it is yet unknown how Brownian motion is influenced by a constantly changing shape. And this is the question that we aim to answer.

In the first chapter of this work, we show how flexible colloidal clusters and chains can be synthesized from spherical colloidal particles using a technique developed by Van der Meulen *et al.*[1] and Chakraborty *et al.*[2]. We describe how the flexibility of such colloidal clusters can be measured and discuss what factors influence the flexibility. We also explore some of the dynamics of flexible colloidal chains.

The second chapter of this work we discuss the Brownian motion of freely jointed colloidal trimers and how this differs from the Brownian behaviour of rigid trimers in various shapes. We first explore the differences in translational and rotational diffusion between rigid and freely jointed trimers. Lastly, we study hydrodynamic correlations between all degrees of freedom of rigid and freely jointed trimers in 2D.
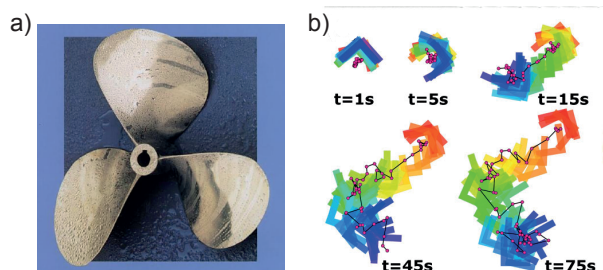

Figure 1: a) Adapted from [3]. Picture of a boat propeller. b) Adapted from [4]. Brownian trajectory of a colloidal boomerang particle.

1 Synthesis and dynamics of freely jointed clusters and chains

Introduction

Multiple studies [1, 2, 5–7] have been done on the preparation of flexible colloidal chains. They have been using two types of bonds between colloidal spheres to form flexible chains; the flexible bond and the freely jointed bond. The difference between these two is that flexible bonds have a preferred bond angle, while freely jointed bonds do not and probe all bond angles with equal frequencies. Both types of bonds are made up of flexible linkers between the colloids, the difference of having a preferred bond angle or not arises from how the linkers are attached to the surface of the colloids. When the linkers are attached at a fixed position on the colloid, as shown in Figure 1.1a, changes in the bond angle are induced by bending of the linkers. Because bending of the linkers increases the energy of the system, the chains prefer to be in their straight conformation, resulting in a so-called (semi-)flexible bond. When the linkers are not attached to a fixed position on the surface and are allowed to diffuse over it, as shown in Figure 1.1b, all bond angles have the same energy and there is no preference in bond angle. This results in a freely jointed bond.

Rigid, semi-flexible and flexible bead-chains can be prepared by binding colloidal particles while they are lined up in an electric[6] or a magnetic[5, 8, 9] field. This technique can be used to produce chains with contour lengths ranging from tens to hundreds of microns.[5] The flexible bond can be established by functionalizing the surface of the colloids and covalently binding linkers between them. Various linkers can be used, including bis-biotin-poly(ethylene glycol)[9] and DNA linkers[5]. The flexibility of the chains can be tuned by varying the length of the linkers[5, 9] and the amount of linkers in a bridge[5]. The latter is dependent on the interparticle distance, which is determined by the strength of the external field.[5, 6] Appropriate field strengths are 0.20 μVm^{-1}[6] when using an electric field and 19–275 G[5] when using a magnetic field. Using long linkers and external field with low strengths result in the most flexible chains.[5]

The freely jointed bond was explored by Van der Meulen *et al.*[1] and Chakraborty *et al.*[2]. They developed a protocol to coat micron-sized particles with a lipid bilayer in which DNA strands with cholesteryl groups could anchor themselves. Because the lipid bilayer is liquid at room temperature, the DNA strands can diffuse through the lipid bilayer and over the surface of the colloid. They functionalized spherical colloids with either DNA strands ending in a type A or a type B of single-stranded sticky ends. When mixing the particles functionalized with the different types of DNA, those with the type A sticky end could bind to those with the type B sticky end when the particles were in close proximity. This system is shown schematically in Figure 1.1b. The linkers spread out over the particle surface when the temperature is above the melting-point of the sticky ends and the linkers accumulate and bind between particles when the temperature

is above this melting point.[1] The reversibility of such systems shows that unspecific interactions between the particles are suppressed by stabilizing polymers that are also anchored in the lipid bilayer.[1] The stiffness of the bond can be increased by increasing the concentration of the DNA linkers in the bonding area.[2] This method to produce freely jointed bonds can be used on particles with various shapes, including spheres, cubes and dumbbels.[2] These can be used to create spherical joints, planar sliders and hinges, in which the shape of the hinges controls the range of motion of the bonded particles.[2]

freely jointed colloidal clusters and chains can also be made with droplets instead of particles.[7, 10, 11] A similar method as the one described above can be used to create freely jointed bonds between droplets. DNA linkers containing cholesteryl groups and a sticky end can anchor themselves in the surface of an oil droplet. This renders the need of a lipid bilayer unnecessary. The mean-squared end-to-end distance and radius of gyration of freely jointed chains with different lengths have been found to scale in good agreement with the Flory theory of a self-avoiding polymer.[7]
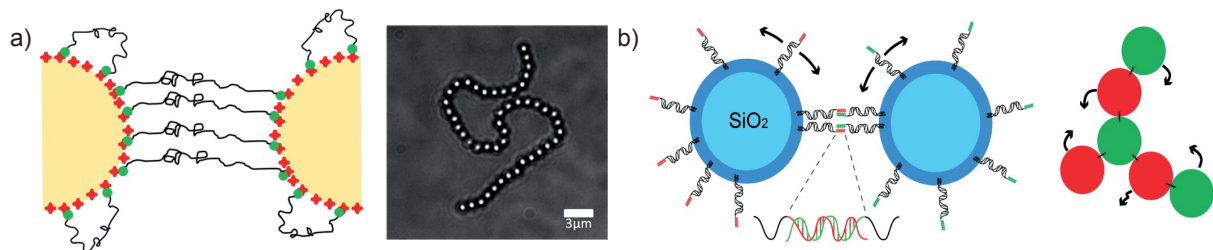

Figure 1.1: a) On the left, a close up of a semi-flexible bond is shown. The DNA linkers are bound on two sides to the functionalized surface of particles, forming a bridge between the two. On the right, an optical microscopy image of a resulting colloidal chain is shown. Adapted from [5]. b) The schematic on the left shows silica particles coated with a lipid bilayer and DNA linkers. The linkers bind the two colloids and a freely jointed bond is formed. The illustration on the right shows the diffusion of the bonds over the surface of particles in a freely jointed cluster. Adapted from [1].

In this project, we set out to produce flexible colloidal clusters and chains. To maximize flexibility and induce larger changes in conformation, we chose to use a freely jointed bond in our system. The freely jointed colloids were produced by functionalizing silica particles of 2 µm with a similar protocol as was established by Van der Meulen *et al.*[1] and Chakraborty *et al.*[2] as mentioned above. In contrast to [1],[2] and [7], we used only one type of DNA linker in our system. The sticky end of our DNA linkers were self complementary to enable binding between all particles and increasing the chance of making longer chains during the formation of clusters.

In this chapter, we first describe how freely jointed clusters can be produced. We then describe how the flexibility of a bond can be measured and we discuss which factors in the experiments can influence the flexibility of the bonds.

Additionally, we show how the same functionalization protocol can be used on superparamagnetic silica particles. These particles can be used for the formation of significantly longer chains in a magnetic field.[5] We also discuss the flexibility of the bonds in these chains and analyze correlations between different joints.

Lastly, we compare the measured mean-squared end-to-end distance of chains with various lengths in our samples to the findings on freely jointed chains made of droplets in [7]. In this paper, the mean-squared end-to-end distance of freely jointed chains made of

droplets were found to scale in good agreement with the Flory theory of a self-avoiding polymer.[7]

1.1 Experimental

1.1.1 Materials

Chemicals

The type A DNA oligomer (Cholesteryl-TEG-5' TTT-ATC-GCT-ACC-CTT-CGC-ACA-GTC-AAT-CTA-GAG-AGC-CCT-GCC-TTA-CGA-TAT-TGT-ACA-ATA-Cy3) and type B DNA oligormer (Cholesteryl-TEG-3'CGT-AAG-GCA-GGG-CTC-TCT-AGA-TTG-ACT-GTG-CGA-AGG-GTA-GCG-ATT-TT) were purchased from Eurogentec. All lipids, 1,2-Dioleoys-sn-glycero-3-phosphocholine (DOPC, >99%), 1,2-dioleoyl-sn-glycero-3-phospho-ethanolamine-N-[methoxy(polyethylene glycol)-2000] (ammonium salt) (DOPE-PEG$_{2000}$, >99%), 1,2-dioleoyl-sn-glycero-3-phosphoethanolamine-N-(lissamine rhodamine B sulfonyl) (ammonium salt) (DOP-Rhodamine, >99%) and 1,2-dioleoyl-sn-glycero-3-phospho-ethanolamine-N-(carboxyfluorescein) (ammonium salt) (DOPE-Fluorescine, >99%) were purchased from Avanti Polar Lipids, Inc. Chloroform ($\geq$99.8%), N-(2-Hydroxyethyl)-piperazine-N'-(ethanesulfonic acid) (HEPES, $\geq$99.5%), 3-(trimethoxysilyl)propyl methacrylate (TPM, 98%), 2-hydroxyethyl acrylate (HEA, 96%), 2-hydroxy-2-methylpropiophenone (darocur 1173, 97%), sodium phosphate monobasic dihydrate ($Na_2HPO_4 \cdot 2\,H_2O$, $\geq$99.0%), sodium phosphate dibasic (NaH_2PO_4, $\geq$99.0%), tetramethylammonium hydroxide (TMAH, 25 wt% in water), tetraethyl orthosilicate (TEOS, $\geq$99.0%) and Pluronic® F-127 (BioReagent) were obtained from Sigma-Aldrich. Sodium chloride (NaCl, ACS, ISO Ph Eur Reagent Grade) was purchsed from Merck, sodium azide (NaN_3, $\geq$99.0%) from Fischer Scientific and ethanol (EtOH, 100%) was purchased from Interchema. Ammonium hydroxide (NH_3, for analysis, 28-30% in water) and hydrochloric acid (HCl, pure, fuming, 37% in water) were obtained from Acros Organics and sodium hydroxide (NaOH, $\geq$99.0%) from VWR International B.V.

Silica (SiO_2) particles of 1.93$\pm$0.05 µm (50 mg/mL in water) and superparamagnetic silica particles containing >25% iron oxide of 0.96$\pm$0.05 µm (25 mg/mL in water) and 2.47$\pm$0.07 µm (50 mg/mL in water) were purchased from microParticles GmbH.

All water used was purified using a NanoPure Milli-Q purification system (MQ, 18.2 MΩ, Millipore).

Equipment

PCR clean Eppendorf tubes and PCR clean pipet tips from Sigma Aldrich were used for all DNA experiments.

A mini extruder set was purchased from Avanti Polar Lipids, Inc. The set was used in combination with filter supports of 10 mm and nucleopore filters with pore size of 0.03 µm from GE Whatman and glass syringes of 250 µL from Hamilton.

The particles were imaged in brightfield with a Nikon Eclipse Ti microscope equipped with a 60$\times$ objective (NA = 0:7) and a Hamamatsu Orca Flash 4.0 camera.

1.1.2   Methods

The DNA linkers were made by hybridization of DNA oligomer types A and B. For this 10 μL of 50 μM oligomer type A and 15 μL of 50 μM oligomer type B were mixed in 90 μL PBS buffer (1 mM NaH_2PO_4, 9 mM $Na_2HPO_4 \cdot 2\,H_2O$, 47 mM NaCl, 3 mM NaN_3 in MQ, HCl and NaOH were used to set the pH to 7.5) and placed in a water bath of 90 ºC for 10 minutes. The bath was then left to cool down slowly to room temperature. The DNA linkers were diluted 10 times in PBS buffer. The composition of the hybridized DNA is shown in Figure 1.2.
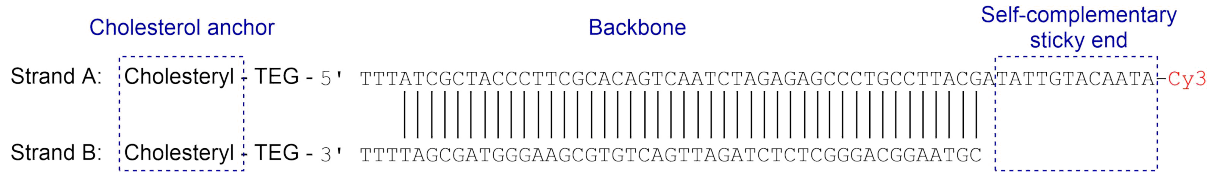

Figure 1.2: Schematic representation of the hybridized oligomers A and B. Both contain a cholesteryl group for anchoring in a lipid phase and a TEG spacer between the cholesteryl group and amino acid sequence. The A strand ends in a self-complementary sticky end. Based on a figure in [1].

To create a film of lipids, 118 μL of DOPC (10 gL^{-1}), 42 μL of DOPE-PEG_{2000} (10 gL^{-1}) and 3.4 μL of DOPE-Flu (1 gL^{-1}) in chloroform were mixed in a glass flask and dried under a gentle N_2 flow. Then 533 μL HEPES buffer (10 mM HEPES, 47 mM NaCl, 3 mM NaN_3 in MQ, pH 7.0) was added, the mixture was placed on a vortex for 30 minutes to form vesicles. The vesicles were pushed through the filters in the mini extruder set 11 times.

30 μL of SiO_2 particles were washed 3 times with MQ before adding them to 30 μL of lipid vesicles in HEPES buffer. The dispersion was placed on a roller shaker system for 1 hour to allow the particles to place themselves in the lipid vesicles. The coated particles were then washed 3 times and redispersed in HEPES buffer. In all washing steps, the particles were centrifuged at 300 g for 4 minutes before removing the supernatant and redispersing in the required medium.

Next, 2 μL of DNA linkers in PBS were added to the vesicle coated particles. The mixture was placed on the roller shaker system for an hour to allow the DNA linkers to anchor into the lipid bilayer. The dispersion was then washed once with HEPES buffer to remove all excess DNA linkers. The dispersions were stored on a roller shaker system. The dispersion was diluted with HEPES buffer for analysis to reduce aggregating of the particles and to improve imaging. Any bonds that might have established during storage were broken before use by heating the particles to 60 ºC and slowly cooling them down to 45 ºC in a water bath. This heating cycle was repeated three times before analysis of the dispersion with the optical microscope.
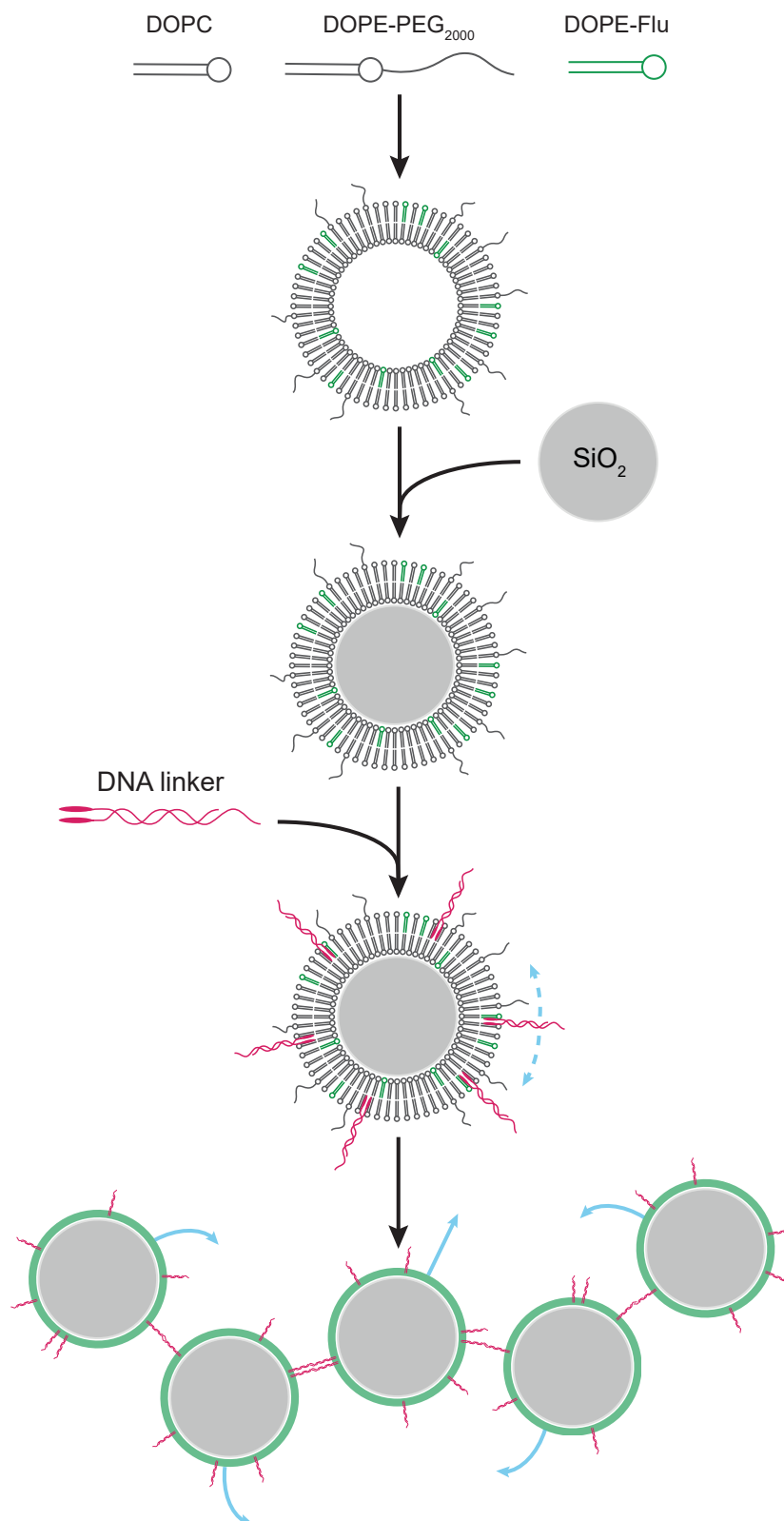
Figure 1.3: Schematic representation of the steps of functionalization of spherical silica colloids with a lipid bilayer and DNA linkers.

Measurement of Brownian motion of the colloids required the particles to be visualized in a drift-free environment. Therefore, cells like the one shown in Figure 1.4 were constructed of a glass microscopy slide with a hole of 18 mm in diameter in the middle, a rectangular glass capillary of 0.1 mm high, 2 mm wide and 5 cm long, blunted needle tips (⌀0.8 mm, Sterican®) and teflon tubing that fit the tips of the needles. The capillary was attached over the hole in the microscopy slide. The plastic of the blunt syringe needles were shortened and the needles themselves were bent 90º. The needles were glued over the ends of the capillary with 2-component expoxy glue. Care was taken to completely seal the gaps between the microscopy slide and the needles, while keeping the ends of the capillary open to the needles. The teflon tubing was attached around the needles to allow easy injection of fluids into the cell.
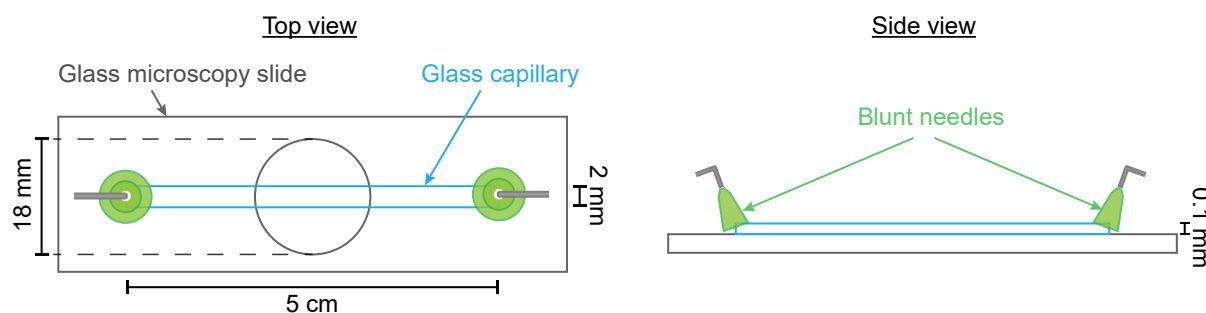

Figure 1.4: Top- and side view of the cells that were used to visualize the colloids in under the optical microscope.

The inside of the capillary was coated with a layer of poly(2-hydroxyethyl acrylate) (pHEA) to prevent the lipids on the colloids of sticking to the glass. For this, the glass capillary was cleaned with 2 M NaOH solution in MQ or in a mixture of MQ and EtOH (MQ:EtOH=1:1) by filling the cell for 5 minutes with 2M NaOH and flushing with MQ when the cell was being used for the first time or by filling the cell for 10 minutes with 2M NaOH in MQ and EtOH for 10 minutes, flushing with EtOH and repeating this three times, when the cell was being reused. The capillary was then rinsed with MQ and EtOH subsequently and filled with a mixture of 800 µL EtOH, 20 µL NH_3 and 20 µL TPM for 1 hour. The capillary was rinsed with EtOH and dried under a gentle N_2 flow. The glass surface was coated with pHEA brushes by filling the capillary with a mixture of 500 µL HEA, 20 µL NH_3 and 20 µL Darocur 1173 and placing it under a long wave UV lamp for 12-15 minutes to polymerize the HEA molecules. The capillary was rinsed with MQ and HEPES buffer before use.
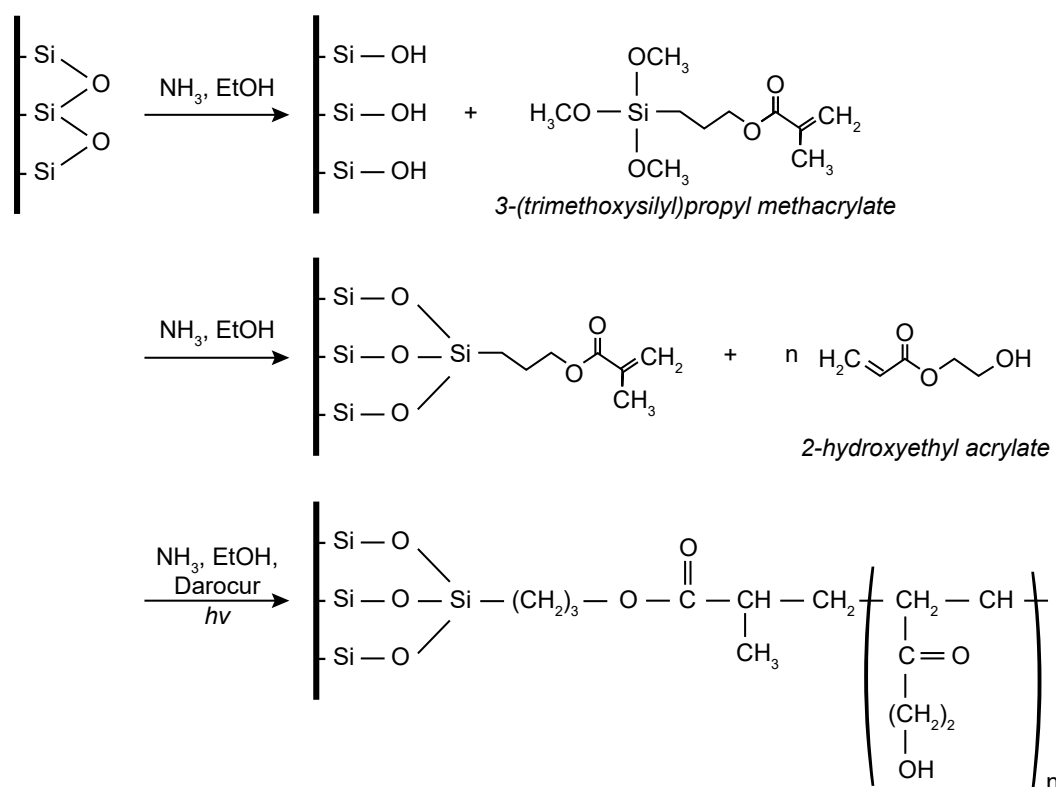
Figure 1.5: The surface of the glass capillary is silanated by addition of TPM in EtOH and NH_3 after which pHEA brushes can be grown on the TPM groups through additive polymerisation.

To make long flexible chains, superparamagnetic silica particles were used instead of regular silica particles. It proved impossible to coat these superparamagnetic particles with a lipid bilayer, this may be due to the presence of iron oxide on their surface. Therefore, superparamagnetic particles were coated with a layer of Stöber silica before coating them with lipid vesicles. The protocol to grow a layer of Stöber silica was taken and adapted from [12]. For the coating of 180 µL superparamagnetic silica particles of 2.47 µm, 17.1 mL EtOH, 2.97 mL MQ and 450 µL TMAH (1 wt% in MQ) were mixed in a 50 mL three-necked round-bottom flask. The particles were washed three times (centrifugation at 200 g for 4 minutes) and redispersed in 900 µL EtOH and sonicated for 30 minutes before adding them to the EtOH, MQ and TMAH mixture. To grow the silica shell, 90 µL of TEOS and EtOH (in ratio 1:1) was added over 45 minutes under constant stirring with and overhead stirrer. The mixture was then stirred overnight to complete the reaction. The coated particles were washed twice in MQ and redispersed in 180 µL MQ and stored on a roller shaker system. For coating these particles with a lipid bilayer and DNA linkers, the same protocol as described earlier was used. These particles had a tendency to stick to the pHEA layer, therefore 5 µL of 5 st% pluronic F-127 in MQ was added to each sample. Long chains were formed by placing the particles in a visualization cell in a magnetic field for 30 minutes.

The gravitational force on the particles confined them to the surface of the glass and the particles were thus always visualized on the bottom of the capillary with the microscope. Because DNA linkers with a self-complementary sticky-end were used for the bonds between the particles, the particles assembled into clusters of varying shapes and sizes. The focus of this project is on flexible linear clusters. Therefore, these were

located and filmed at 5 frames per second (fps) for about 30 minutes or as long as the particle stayed flexible and did not stick to the surface of the capillary. The gravitational height of the 2 μm SiO$_2$ particles is 62 nm, using $h_g = \frac{k_B T}{\frac{4}{3}\pi a^3 \Delta \rho g}$ with T = 298 K, $\rho_{H_2O} = 997$ kgm^{-3} and $\rho_{SiO_2} = 2600$ kgm^{-3}.[13–15] Therefore, the recorded motion of the particles was essentially in 2D.

The positions of the particles could be extracted from the videos using a Matlab implementation of Crocker and Grier [16]. The distances between all particles were determined and used to determine which particles were neighbours to each other, enabling us to extract all linear clusters and chains.

1.2   Results and Discussion: freely jointed trimers

The resulting clusters were observed with an optical microscope. A time series of a flexible trimer can be seen in Figure 1.6, in which the conformational change of a trimer over 35 seconds is shown with time steps of 5 seconds. The trimer is able to fold up to a triangle, stretch out and fold up in the other direction. These are all conformations with an internal angle between $\alpha = -0.67\pi$ radians and $\alpha = +0.67\pi$ radians that a freely jointed trimer consisting of hard spheres should be able to probe. How α is defined is shown in the image at t=0 s in Figure 1.6.
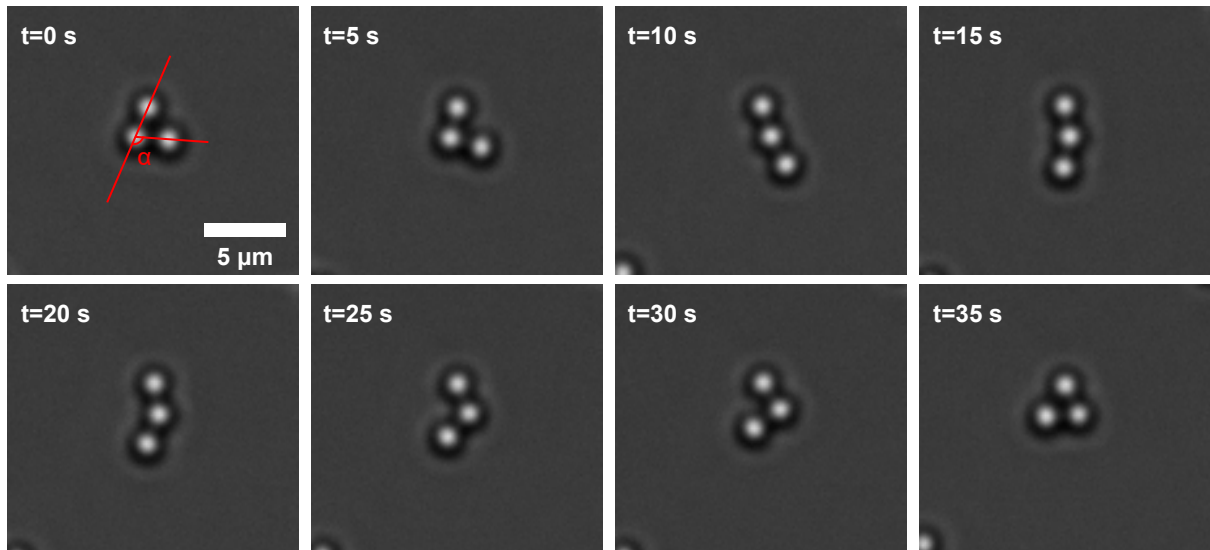
Figure 1.6: Timeseries of a flexible trimer over 35 seconds. How the internal angle α is defined is shown in the image at t=0 s. The trimer probes all internal angles α that are possible for a freely jointed trimer consisting of hard spheres.

1.2.1   Character of the bonds

The positions of the particles were determined in all frames to determine whether the established bonds were indeed freely jointed. The measured positions could be used to determine the internal angle (α) of the trimers in each frame. Figure 1.7 shows that α is defined as the angle between the line going through the center of the middle particle (particle 2) and the particle on its left (particle 1) and the line through the middle particle and the one on its right (particle 3). If a trimer is freely jointed, particle 3 is able to make

a complete circle around particle 2 when particles 1 and 2 are fixed with their centers on a horizontal line, except for the positions where it encounters particle 1. Figure 1.7b shows all positions that the center of particle 3 could reach in one of the synthesized trimers. The warm colours indicate positions where the particle is more often found and the cold colours indicate positions where the particle is seldom found. The angles at which particle 3 encounters particle 1 are indicated with red lines. The figure shows that all expected positions are probed, although not with exactly the same frequency. The upper half of the circle is probed more often than its lower half. This effect is expected to disappear and all angles will be probed equally often if this figure is made for a series containing more frames, because the angle histogram in 1.7c is quite flat. The angle histogram in Figure 1.7c shows how many times all angles α were measured in 14 flexible trimers. The histogram is almost flat, showing that the established bonds do not show a preferred angle and are truly freely jointed.
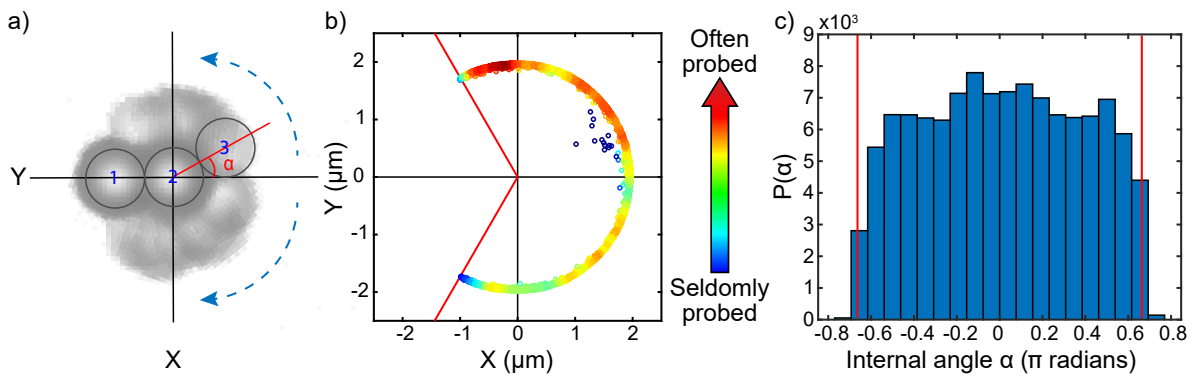

Figure 1.7: (a) Reduced tracks. The positions marked with warmer colours are probed more often than those of colder colour. The particles diffuse nicely over the whole circle. (b) Angle histogram including angles of 14 flexible trimers. (c) Mean-squared angular displacement versus time.

1.2.2 Measuring flexibility

The flexibility (J) of a bond is defined as the speed at which α changes. This can be determined by measuring the mean-squared angular displacement (MSAD) of the internal angle as a function of time. The principle of the MSAD is very similar to the mean-squared displacement (MSD), which is a well-known measure for the displacement of a Brownian particle. In this section, MSD is discussed and used to explain how the MSAD can be used provide a way of quantifying the flexibility of freely jointed bonds.

Let's first consider a one-dimensional system of a particle exhibiting Brownian motion on a line, like the one shown in Figure 1.8a, of which we want to know how fast it is moving. According to Newton's second law, the speed of an object is defined as

$$v = \frac{s}{t} \tag{1.1}$$

with v the speed, s the distance the particle is traveling and t the time. This is straightforward for an object moving in ballistic motion. But a colloidal particle only moves ballistically on a time scale of $\propto 10^{-10}$ s. Its mean displacement on longer time scales is not an appropriate measure because the particle is performing a random walk. This

means that the particle will move to the left (-1) as often as to the right (+1) and averaging these steps will always result in a net displacement of zero. Therefore, the mean displacement is not a good measure to use in determining how fast a Brownian particle diffuses. This can be remedied by squaring all steps before taking their mean. This removes all negative values, resulting in a non-zero mean-squared displacement (MSD) that can be used to determine the diffusivity of the particle. The MSD can be calculated using equation 1.2 with $x(t)$ the displacement at a time t and x_0 the displacement at time $t = 0$.[17]

$$\langle x^2 \rangle = \langle (x(t) - x_0)^2 \rangle \tag{1.2}$$

Which is related to the diffusion coefficient through the Einstein equation for the average quadratic displacement through equation 1.3.[18]

$$\langle x^2 \rangle = 2D_T t \tag{1.3}$$

With D_T the translational diffusion coefficient of the particle. This equation results in a linear function of time in the diffusive regime of the particle, with a slope of $2D_T$. This means that the length of the excursions that the particle makes, increases linearly with time. The measured MSD of a spherical colloid is plotted in Figure 1.8d. As this particle is diffusing in two dimension, the slope is equal to $4D_T$ instead of $2D_T$. Now, using Newton's second law 1.1, the slope of this graph directly yields a measure for how fast the particle is exploring its surrounding area.

Next, we consider a particle that is performing a random walk on a line that has been folded around to form a circle. The path that the particle is exploring can then be translated into angles instead of distances, as shown in Figure 1.8b. And the MSD can be translated into a mean-squared angular displacement (MSAD).

A similar approach can be used when describing the MSAD of the internal angle α of a freely jointed trimer. The edge particles of a freely jointed move on a circle around the middle particle as shown in Figure 1.8c. In this figure, α is defined as described previously in section 1.2.1 and changes with each random step the particles on the circle take. The changes in α then harness information on the random walks that both particles on the circle are performing and their individual MSADs can be combined to one. When the MSAD of α is plotted against time, as can be seen in 1.8e, it starts out quite similar to the graph of MSD against time (Figure 1.8d). The MSAD of α increases linearly at a short timescale, but it changes quite dramatically on longer timescales where the slope decreases and the graph eventually plateaus. This maximum MSAD is caused by the range of angles that α can be. This range of α is limited to angles between -0.67π radians and $+0.67\pi$ radians. These are the angles where the particles on the circle encounter each other. Therefore, α cannot change more than the full range between -0.67π radians and $+0.67\pi$ radians, corresponding to an MSAD of 4.4 rad^2. The flexibility of the bond is defined as the rate at which the MSAD of α is changing. As the slope is different at different timescales, we use the initial slope of the MSAD as a measure for the flexibility of the bond.
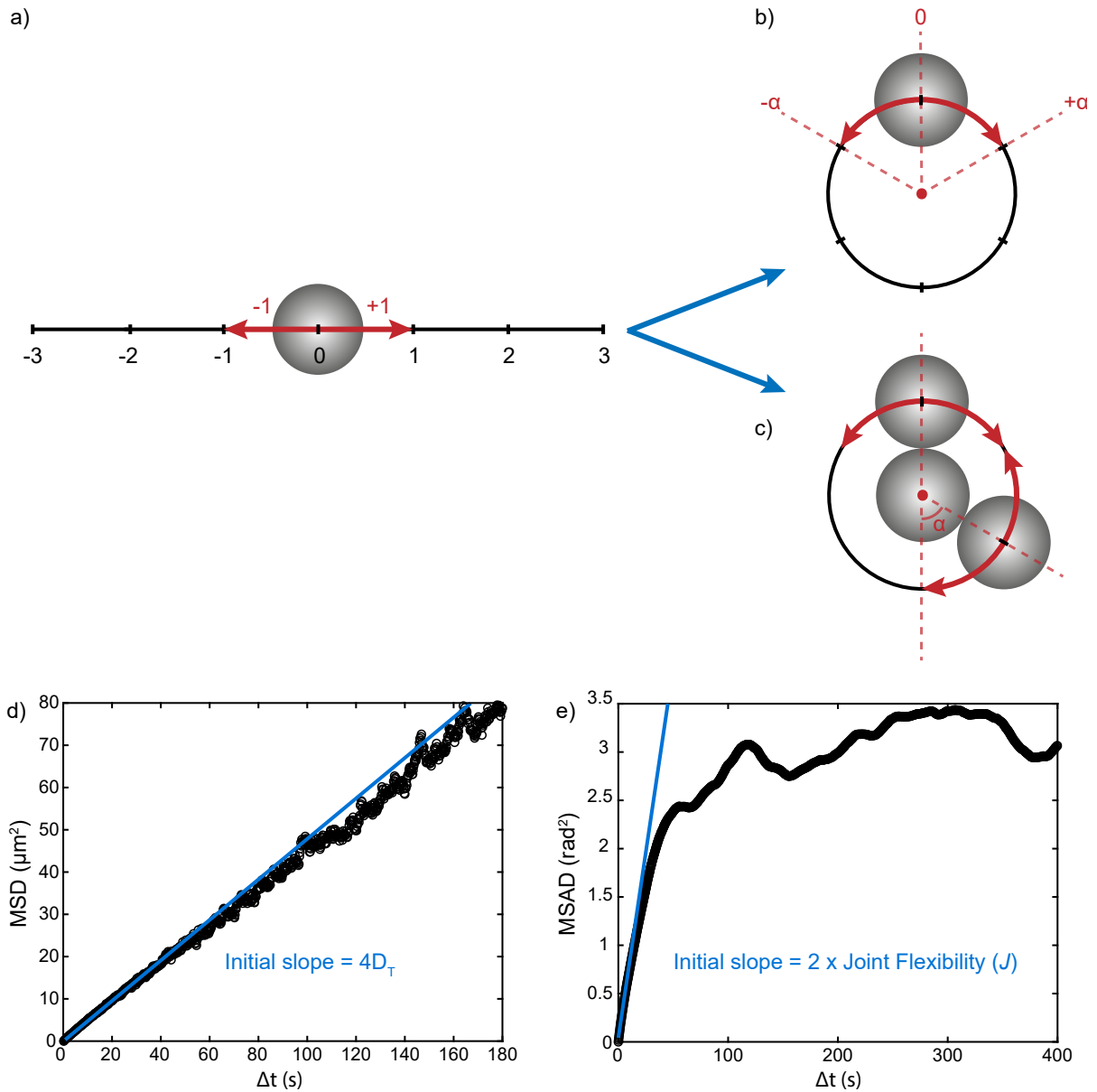
Figure 1.8: a) Particle performing a random walk on a line can also be confined to a circle, the random walk can be translated from distances to a the change in internal angle of a trimer. This gives the mean-squared angular displacement. b) MSD plotted against time for a sphere confined in 2D. c) MSAD of the internal angle of a flexible trimer plotted against time.

1.2.3   Influences on flexibility

The flexibility of each produced freely jointed trimer was determined by measuring the MSAD of α as a function of time and its initial slope, as described above. All measured values were between 54 and 177 $\deg^2 s^{-1}$ with an average flexibility of 117.2±26.0 $\deg^2 s^{-1}$. The distribution of these values is visualized in the histogram in Figure 1.9 with the joint flexibility on the x-axis and the amount of trimers found with that flexibility on the y-axis.

Because our system is quite complex, there are several variables that could influence the flexibility that we measured for each individual trimer, causing this distribution in

measured flexibility. In this section, we discuss some of these factors. The DNA linker density is known to have a great influence on the flexibility of the freely jointed bonds[2], this will be discussed in detail in section 1.2.4.
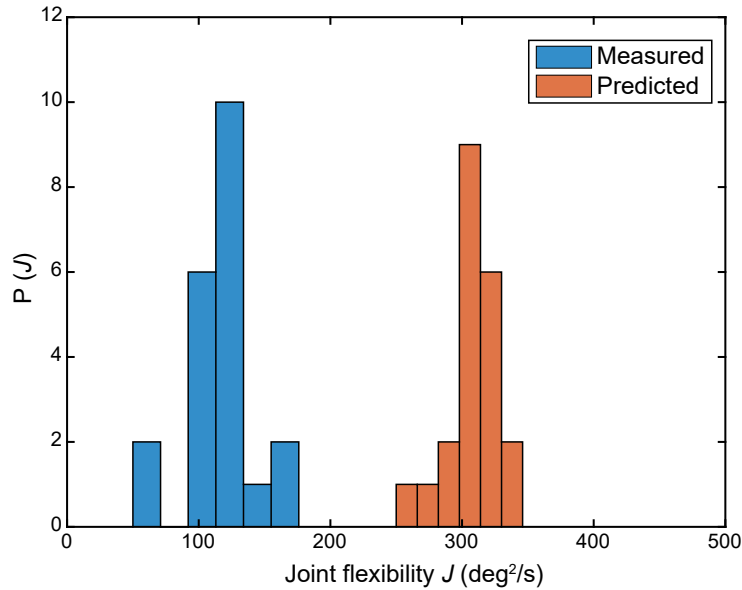

Figure 1.9: Histogram of measured flexibilities of all flexible trimers.

Poly-2-hydroxyethyl acrylate layer

One of the factors influencing the observed flexibility of the freely jointed clusters is a fluctuation in the thickness of the pHEA layer on the surface of the glass capillary. This is because a thicker pHEA layer may increase the drag that a trimer experiences during its random walk.[2] To investigate whether the observed spread in measured flexibility was caused by fluctuations in the pHEA layer between all samples, for each trimer included in Figure 1.9, a monomer was found and tracked in the same sample and thus under similar experimental conditions. The MSD of each monomer was translated to a MSAD by converting its track to a circular motion with a similar radius as the particles in a trimer are diffusion over. From these MSADs the 'flexibilities' of the monomers could be determined. These values are also included in the histogram in Figure 1.9. These values also represent the predicted maximum flexibility that a trimer could exhibit. All predicted values were between 258 and 343 $\deg^2 s^{-1}$ with an average flexibility of 311.5±20.9 $\deg^2 s^{-1}$, corresponding to an average translational diffusion coefficient of 0.091±0.009 $\mu m^2 s^{-1}$.

The spread in predicted flexibilities is similar to the spread in measured flexibilities, indicating that it is caused by slight fluctuations in the experimental conditions. However, the samples in which the most flexible trimers were found did not necessarily contain the most mobile monomers. Therefore, we concluded that the pHEA layer did not vary greatly between samples.

For SiO_2 spheres of 1.93 μm in diameter, the Stokes-Einstein equation

$$D_T = \frac{k_B T}{6\pi\eta a} \tag{1.4}$$

gives a translational diffusion coefficient of 0.25 $\mu m^2 s^{-1}$, when T=298 K, η is the viscosity of water and a=0.965 μm. This is more than twice the diffusion coefficient that was

measured for the monomers in our samples. This decrease in mobility is caused by the pHEA layer and the proximity of the glass surface.[18] Both these factors can increase the drag on the colloids when comparing with colloids suspended in a homogeneous aqueous environment where no walls and polymer layers are present. We can conclude that the pHEA layer does influence the diffusion of the particles, nevertheless it is quite a constant effect.

Bonds

Figure 1.9 shows that binding the monomers to each other slows their diffusion down even more, as all predicted flexibilities are evidently higher than the measured values for trimers. This is caused by two extra factors that are introduced when establishing the freely jointed bond between the particles. The first factor that is introduced is drag of the DNA linker patch in the lipid bilayer on the surface of the colloids.[1, 2] This will be discussed in more detail in section 1.2.4. The second factor that we consider is the drag of the particles on each other caused by bringing the particles in close proximity of each other. This effect is expected to be quite constant in all trimers and it is expected to be larger in larger clusters in which there are more bulk particles enclosed by two neighbouring particles.

Storage time

The last factor for which we determined its influence on the flexibility of the trimers is the time between completion of the functionalization of the particles and the moment the trimers were observed and filmed under the microscope. This time ranged between 23 and 71 hours. Optimally, the lipids and DNA oligomers should be stored at -20°C. Yet after functionalization of the colloids, they were stored on a roller shaker system at room temperature to prevent sedimentation and aggregation of the colloidal particles. This can affect the quality of the lipids and DNA linkers. To investigate whether the storage of lipids and DNA linkers was affecting the flexibility of the clusters, the joint-flexibility was plotted against the storage time in Figure 1.10. The different symbols and colours indicate different batches of functionalized colloids that were prepared in the same way. At all storage times, large variations in measured flexibilities are observed inside both batches. The two batches combined do not show a clear trend either. Therefore, we do not consider the amount of time that the samples are stored outside the freezer as an important influence on the flexibility of the trimers.
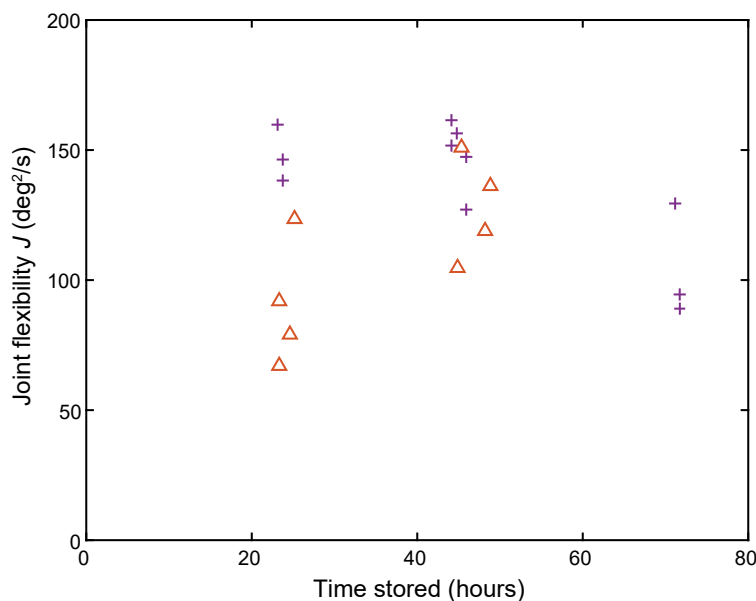
Figure 1.10: Graph showing measured flexibility of trimers against the time the sample had been stored at room temperature. The different colours and symbols represent different batches of freely jointed trimers, they were produced using the same protocol. No correlation is found in these data.

1.2.4   Tuning flexiblity

Chakraborty *et al.*[2] reported a clear dependence of joint flexibility on linker density in the DNA linker patch. They determined the linker density in the bond area with confocal microscopy. As shown in Figure 1.11a, Chakraborty *et al.* found that there was no bonding when the DNA linker density was below 10^3 linkers μm^{-2} and only rigid bonds when the DNA linker density was above about 1.1×10^4 linkers μm^{-2}. They concluded that bonds form rapidly enough while obtaining an adequate joint flexibility at a linker density that lies roughly between $10^3 - 10^4$ linkers μm^{-2}.[2]

We set out to use these findings to optimize the flexibility of our system by varying the amount of DNA linkers that were added to the samples and comparing the flexibility of the resulting clusters. The flexibility of at least two resulting trimers was measured in every sample. The maximum amount of DNA linkers on the surface of each colloid μm^{-2} was used as a measure for the linker density. We assumed that all added DNA anchored itself the lipid bilayers on the colloids during synthesis and that the DNA linkers were evenly distributed over all colloids. This experiment was performed for four batches of functionalized colloids, which were produced in the same way. The results are shown in Figure 1.11b, with the different colours and symbols representing the four different batches. The graph shows a large spread in flexibility at the same assumed DNA linker density. The variation in flexibility of freely jointed trimers at the same maximum DNA linker density was so large that no correlation could be found between the added amount of DNA linkers and the flexibility of the resulting clusters. Therefore, we did not manage to tune the flexibility of the clusters by changing the total amount of DNA linkers that were added to the samples.

In addition to a clear dependence of flexibility on the DNA linker density, Chakraborty *et al.* found that the DNA linker density on colloids varies greatly within a sample.[2]

This is in line with our difficulties in tuning the joint flexibility of clusters. The variation in flexibility within a sample is probably due to variation in the actual linker density on the colloids in our samples. We can conclude that the assumption that the DNA linkers that are added to the sample are distributed evenly over all particles is not correct.
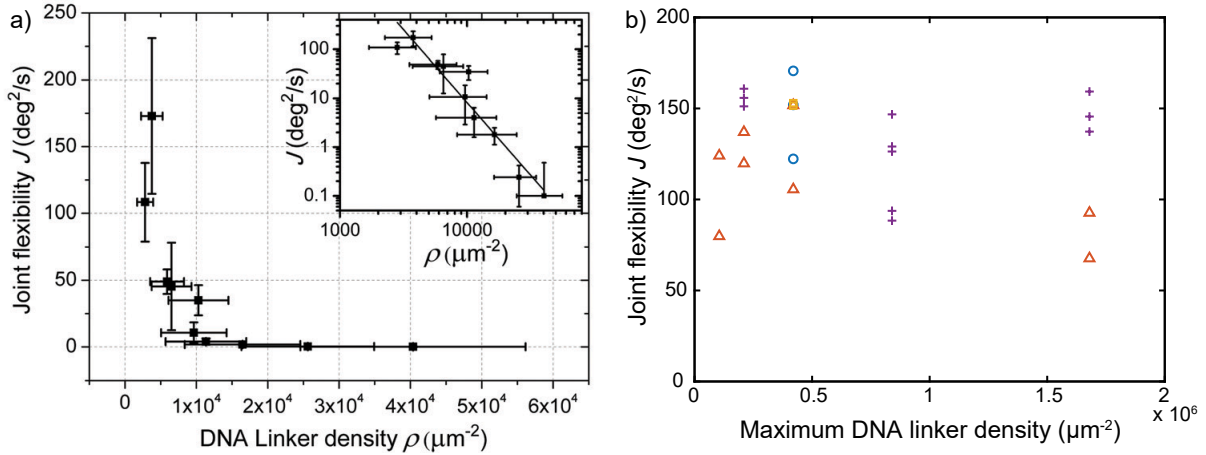

Figure 1.11: a) Graph showing the dependence of joint flexibility on the DNA linker density in the linker patch, found by Chakraborty *et al.*. Adapted from [2]. The graph shows a clear minimum of linker density below which no bonding was observed between the colloids, a clear optimum linker density and a sharp decrease in flexibility if the optimum linker density is exceeded. b) Determined flexiblities of clusters in our samples as a function of theoretical DNA linker density per surface area. The different colours and symbols represent different batches, which were produced in the same way and analyzed in similar conditions. There is no trend in these data points.

Accumulation of DNA linkers in bond area

Van der Meulen *et al.*[1] showed with confocal microscopy that the mobile DNA linkers accumulate at the interparticle contacts below the sticky end melting temperature. We were able to observe the influence this process on the flexibility of the trimers. This was done by filming a flexible trimer for 20 hours and determining its flexibility over every hour. The results of this experiment are shown in the graph in Figure 1.12a. This graph shows a clear decrease in flexibility over the first 5 hours after establishment of the bond. The flexibility decreases very slightly after this and remains at around 90 $\deg^2 s^{-1}$ for the remainder of the movie. The flexibility decreases sharply at t=8 and t=13 hours, but recovers to its original trend rapidly. This is probably caused by temporary sticking of one of the particles to the pHEA layer on the surface of the capillary.

Our data show nicely the combination of the accumulation of the DNA linkers in the binding area and the effect it has on the flexibility of the bond. The decrease in flexibility is caused by an increase the drag of the linker patch in the lipid membrane with the accumulation of the linkers in the bond area.[1, 2] To illustrate this, a cartoon is included in the Figure 1.12a, showing a single bond between two particles and multiple unbound linkers diffusing over the remaining surface of the particles at the start of the measurement. And the same particles after the flexibility of the bond has reached its minimum and a maximum amount of linkers has diffused towards and joined the linker patch. This maximum number of linkers may be limited either by the amount of linkers

present in the membrane; when all linkers have accumulated in the bond area, the density cannot increase any more (shown in Figure 1.12b). Or by the length of the DNA linkers; when the distance between the surfaces of the two particles is too large for the linkers on either side to reach and bind each other, they may leave the bond area (shown in Figure 1.12c).

The flexibilities of all other trimers were measured intermittently in the first 4 hours after establishment of the bonds. This is the time in which the flexibility is still decreasing and has not stabilized yet in Figure 1.12a. This may contribute to the spread in flexibilities that was seen in Figure 1.9. This also explains why the flexibilities that were measured in section 1.2.4 were generally higher than the flexibility that this particle stabilizes at. If the joint flexibility at maximum accumulation of the DNA linkers in the bond area is limited by the amount of linkers on the particle surface, as shown in Figure 1.12b, the graph in Figure 1.11 may improve when joint flexibility is determined after more than 6 hours after injecting the sample into the visualization cell. We hypothesize that the particles in samples to which more DNA linkers have been added will stabilize at a lower joint flexibility than the clusters in the samples to which fewer DNA linkers have been added.
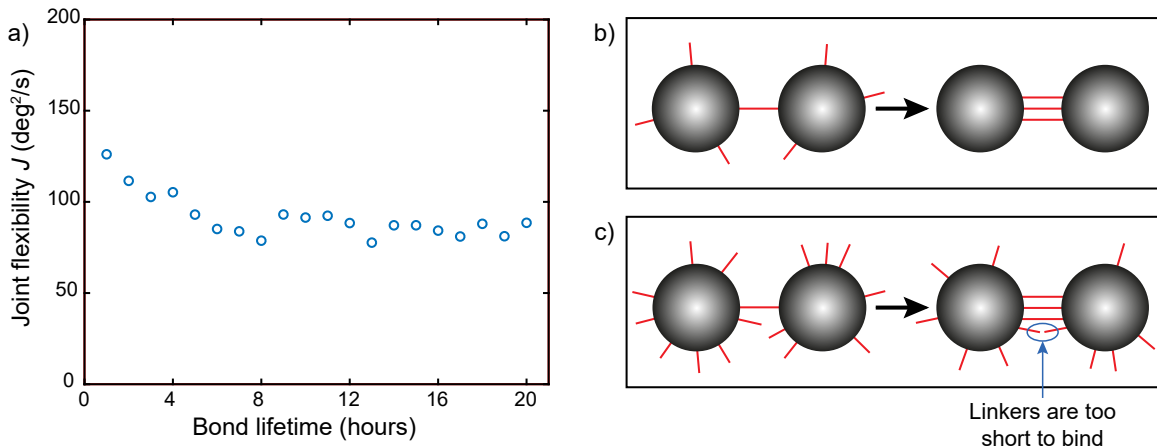

Figure 1.12: a) Flexibility of a freely jointed trimer as a function of time over 20 hours. b) Schematic of DNA linkers on the particles accumulating in bond area over time. When all linkers have bound in the linker patch, the patch cannot grow any further. c) Schematic of DNA linkers on the particles accumulating in bond area over time. The growth of the linker patch is limited by the length of the DNA linkers. The linker patch is limited to the area where the interparticle distance is small enough for the linkers to reach each other.

1.2.5   Bond breakage

Occasionally, bonds in clusters in our system were observed to break. This has been recorded to happen to multiple trimers that have been intact for various amounts of time. These breaking events seem to occur more often in samples to which relatively low amounts of DNA linkers have been added. Breaking events also occurred more often in samples to which a blocker for the self-complementary sticky end was added.

It is unlikely that breaking is caused by the DNA linkers detaching from the lipid membrane because the linkers posses a double cholesterol anchor that makes the attachment of the linkers to the membrane essentially irreversible.[1] That bond breakage

happens more often in samples in which a blocker for the sticky end is present suggests that it is dehybridization of sticky ends that causes the bonds to break. We suspect that the presence of the blocker weakens the bond between the DNA linkers.

We suspect that bond breakage is caused by the implementation of a different sequence in the sticky end of the DNA linkers because this is the main difference between the system used in this project and in projects in which no breaking events were observed. The sticky end of the DNA linkers used by Van der Meulen *et al.*[1] and Chakraborty *et al.*[2] have similar lengths (12 base pairs) and melting temperature (55 °C, [1]) as in this project. They both used two types of DNA linkers instead of one with a self-complementary sticky end. Therefore, we suspect that it is the introduction of the self-complementary sticky end that causes bond breakage.

We managed to record bond breakage in some clusters as sticking events. All particles in our system can bind to each other when they are in close proximity of each other. Therefore, the edge particles of a trimer can bind to each other when the trimer is in its most compact conformation. In most cases, the cluster stays like this permanently. Such clusters were occasionally observed to unfold again, restoring the cluster's flexibility. This can clearly be visualized when the internal angle α is measured and plotted through time. Figure 1.13 shows such a plot for a freely jointed trimer. In this graph, two plateaus are visible, the first (indicated with a red circle) starting at t=703 s where the edge particles bind to each other for 39 seconds and the second from t=1660 s to the end of the movie at t=1798 s. The first plateau shows that the edge particles are able to release each other after having been bound for more than half a minute.
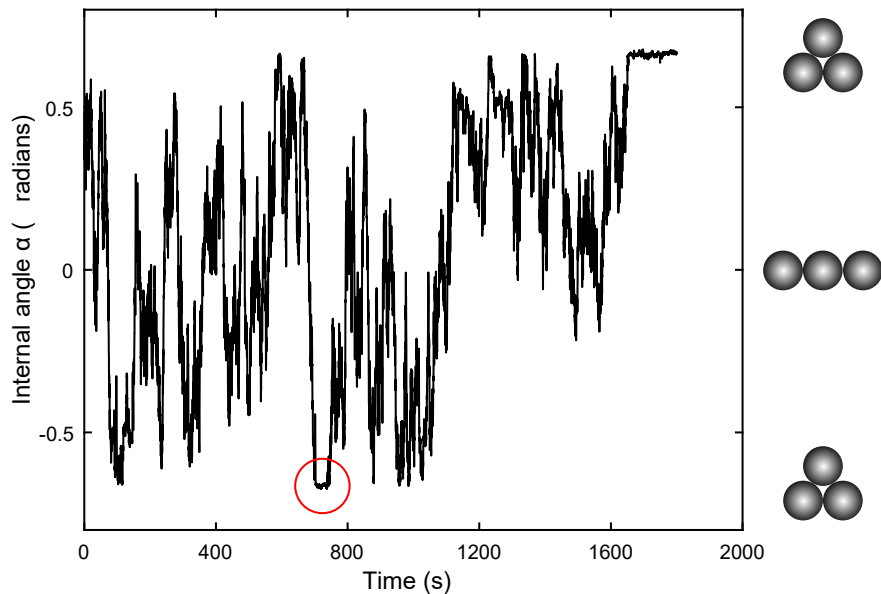
Figure 1.13: Graph showing the internal angle α through time. The angle fluctuates between $+0.67\pi$ radians and -0.67π radians as expected. Plateaus are sometimes observed at the maximum and minimum angles where the outer particles encounter and bind to each other. This bond is permanent in most cases, but has occasionally been observed to break after some time. Such a temporary bond is visible in this graph and indicated with the red circle.

1.3   Results and Discussion: freely jointed chains

In this section, we first examine whether the coating of superparamagnetic colloids with SiO_2 has been succesfull. We then address the stability of the chains and possible causes for occuring bond breakage. And lastly, we briefly discuss hydrodynamic correlations within the flexible chains that we produced.

1.3.1   Silica coating

The superparamagnetic particles were coated with Stöber SiO_2 to assure that the particles could be coated with a lipid bilayer and DNA linkers. Scanning electron microscopy (SEM) images were taken to confirm that coating of the superparamagnetic particles with SiO_2 had been successful. These images can be seen in Figure 1.14. From these images the size of the particles before and after coating with SiO_2 were determined at 1.97±0.08 μm and 2.36±0.09 μm respectively, showing that a SiO_2 layer of 0.20±0.04 μm has successfully been grown onto the particles. Small protrusions can be seen on the SiO_2 coated particles, making their surface slightly rougher.
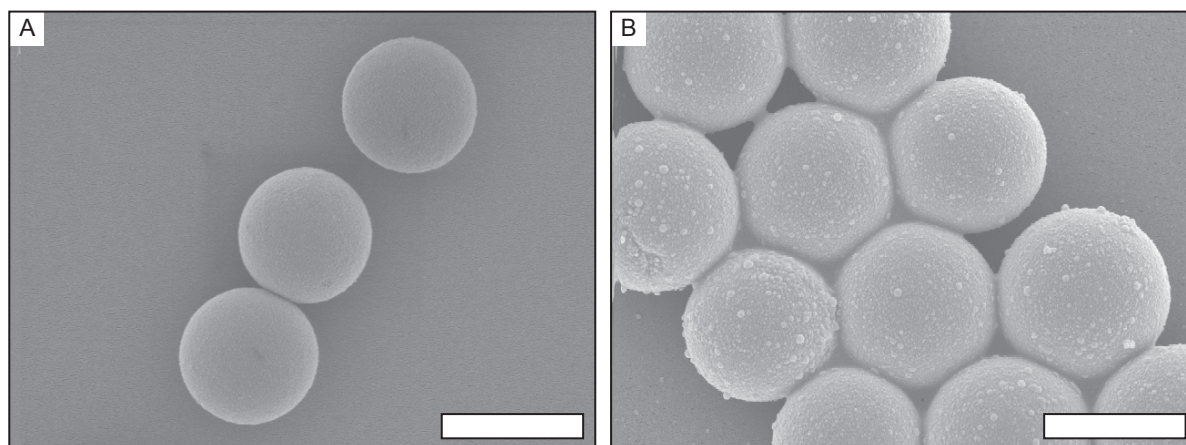

Figure 1.14: SEM images of iron oxide containing SiO_2 particles before (A) and after (B) coating with Stöber SiO_2. The scale bars represent 2 μm.

1.3.2   Bond breakage in chains

After functionalization of these particles with a lipid bilayer and DNA linkers, the para-magnetic particles were lined up by placing them in a magnetic field (produced with Geomag permanent magnets placed parallel on either side of the capillary), as shown in the optical microscopy image at t=0 in Figure 1.15. Keeping the particles lined up for 30 minutes allowed the DNA linkers on their surfaces to bind to each other, creating colloidal chains. The diffusion of these chains can be seen in Figure 1.15. In the figure can be seen that the chains are able to bend and flexible bonds have formed. Figure 1.15 also shows that the chain breaks at multiple positions immediately after removal of the magnetic field. From this, we can conclude that some particles do not establish any bonding with the particle next to it. This problem may be caused by either insufficient time for the DNA linkers to encounter and bind to each other. If this is the case, lining the particles up for longer than 30 minutes should result in longer chains. Or from a deficiency of DNA linkers on the surface of one of the particles, rendering the particle unable to establish

bonds with the particles on both its sides and ending the chain. This should be resolved by adding more DNA linkers on the surface of the colloids. This solution increases the risk of binding of particles inside one chain, transforming the linear chains to random clusters.
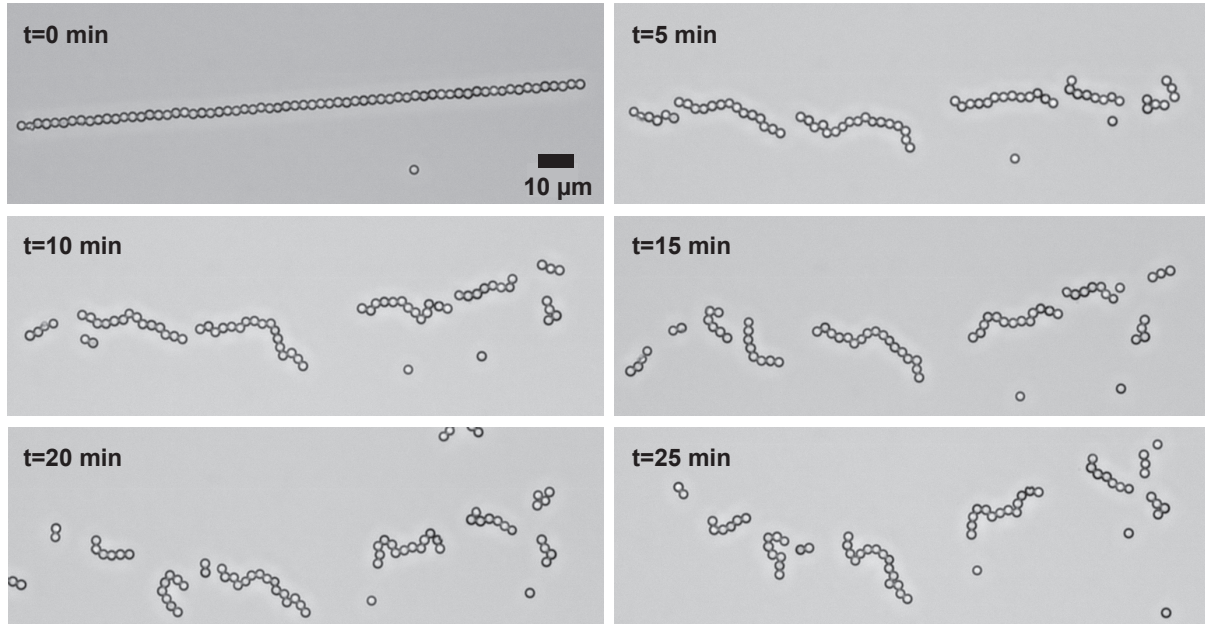

Figure 1.15: Time series of a freely jointed chain made up of iron oxide containing SiO_2 particles after 30 minutes of being lined up in a magnetic field. Particles at multiple positions in the chain have not established bonds with both their neighbours.

The bonds have also been observed to break later in time. Figure 1.16 shows this more clearly. It shows a chain from t=0 at which the particles were lined up in a magnetic field, to t=25 minutes after removal of the magnetic field with breaking events after 10 to 20 minutes after removal of the magnetic field. The first bond breaks at t=10 minutes and the second at t=20 minutes after which no further breaking has been recorded. This is remarkable because DNA linkers are expected to accumulate and bind in the bond area[1] and strengthen the initially established bond. That the freely jointed bonds can break was also noticed earlier in trimers, as described in section 1.2.5. The breaking events in the samples containing superparamagnetic particles can be caused by the addition of pluronic F-127, that was added to prevent the particles from sticking to the pHEA layer. This is suspected because Rinaldin *et al.* reported that pluronic F-127 is able to release the anchored DNA linkers from a lipid bilayer in a similar system to ours.[19] As no pluronic F-127 was added to the samples containing regular SiO_2 particles, breaking events in those samples must have a different cause.

Figure 1.17a shows an image of the the 22 particles long chain which was intact at t=10 minutes together with a graph of the flexibility of its bonds as a function of bond number. The flexibility of the bonds in the chains was determined in the same way as for the flexible trimers. Because the flexibility of the bonds cannot be directly measured, but the angle between three particles must be analyzed instead, the position of the bond was defined as the middle particle of the triplet forming the measured angle. This assignment of the bond numbers is shown in Figure 1.17c. The positions where the chain broke have been indicated with dashed red lines both in the image and the graph. The chain breaks first between α_4 and α_5, then between α_5 and α_6. The first breaking event created a

pentamer, which also broke later in time. Its bond flexibility and position of breakage are shown in Figure 1.17b.

　　Both figures show a large fluctuation in flexibility inside the chain and breaking in the most flexible bonds. The sixth particle in the chain in Figure 1.17a is the center of the most flexible angle (α_5) and completely escapes from the chain, which indicates that the DNA linker density on the surface of this particle is lower than on the other particles in the chain. This could be investigated further with fluorescence measurements for a more certain conclusion.

Another striking detail in Figures 1.17a and 1.17b is the difference in flexibility of α_1 and α_2. They indicate the bonds between the same particles in both graphs, but their determined flexibility in Figure 1.17b is about half of what it was in Figure 1.17a. This shows that these bonds become more rigid after the pentamer has separated itself from the large chain.
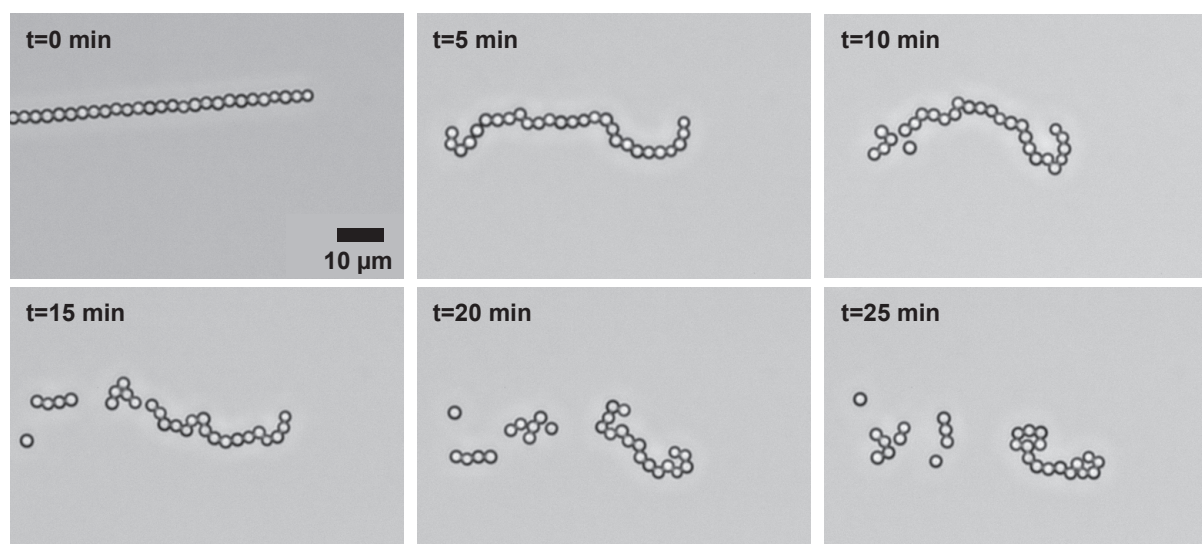

Figure 1.16: Time series of a freely jointed chain made up of superparamagnetic SiO$_2$ particles after being lined up in a magnetic field for 30 minutes. The series shows some bonds breaking after having been bound for 5 or 15 minutes.
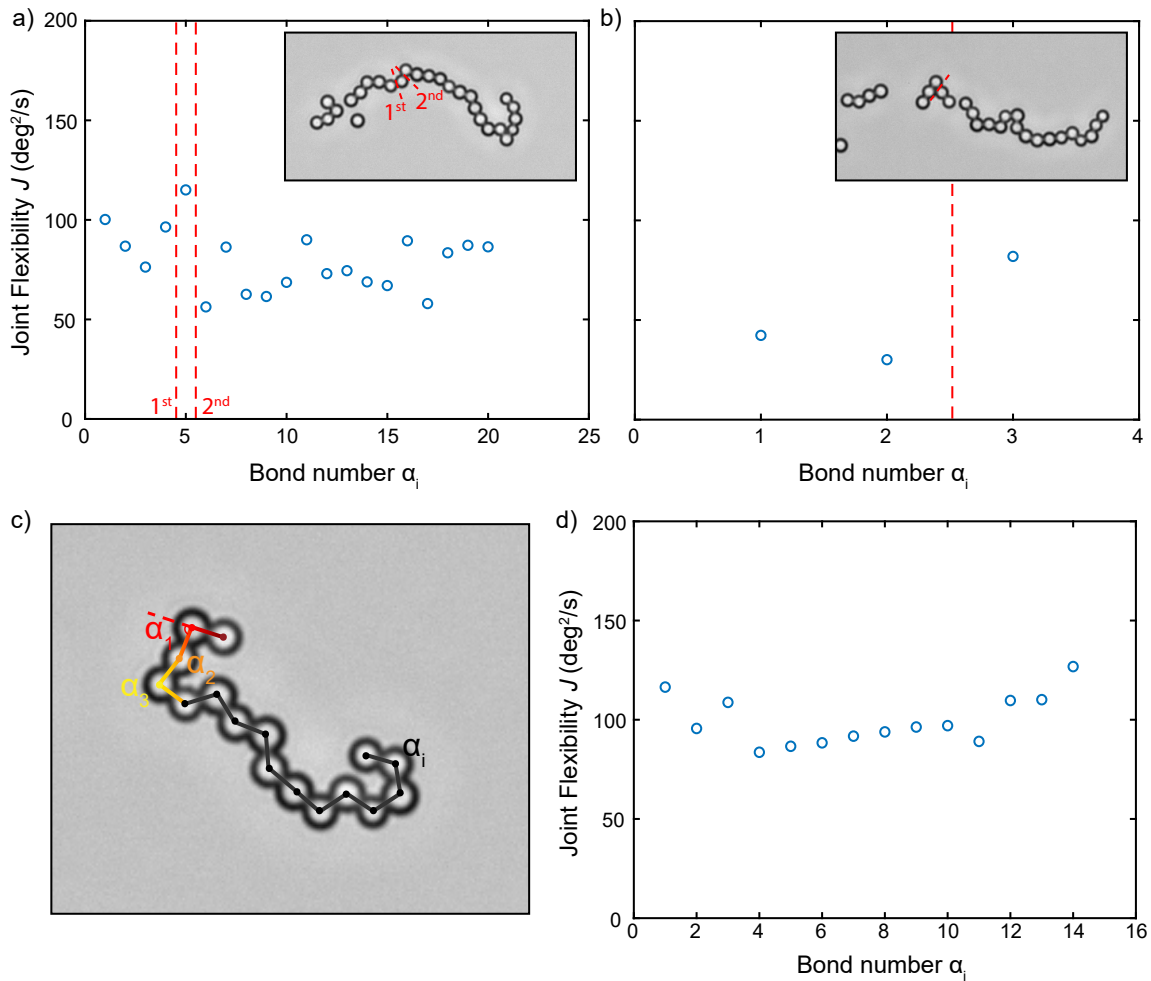
Figure 1.17: a) Image of a freely jointed chain of 22 particles long that will break later in time. The flexibility of each angle has been plotted to the corresponding bond number (α_i). The breaking bonds have been indicated in the image and the graph with dashed red lines. b) A similar figure for the pentamer created by breaking of the first bond. c) A freely jointed colloidal chain. All angles between three particles can be measured and are labeled α_1 to α_i from one end of the chain to the other. d) Graph showing the flexibility of the bonds of the chain in figure c) as a function of bond number.

After 20 minutes, no more breaking events were recorded. The flexible chain of 16 particles long that was left after all breaking events stayed intact for more than another 30 minutes and was tracked and analyzed. The flexibility of each bond has been plotted against the bond number in the chain in Figure 1.17d. This figure shows that all bonds in this chain have a flexibility of at least 86 $\text{deg}^2\text{s}^{-1}$ and that the flexibility of the bonds decreases as the distance to the chain end increases. Showing us that the position in the chain influences the flexibility of the bond. This is as expected, because more particles have to move to induce a change in an angle in the middle of the chain than in an angle towards the end of the chain. This is in agreement with the observation that the bonds in the middle of a longer chain of 22 particles long have lower flexibilities (see Figure 1.17a) than those of the 16 particles long chain.

Additionally, if it is true that the first and last particle form the ends of the chain because of too low an amount of DNA linkers on their surface to bind two particles, they will have fewer DNA linkers in their DNA linker patch, resulting in a more flexible bond.

1.3.3   Hydrodynamic correlations

We studied correlations between changes in internal angles at different positions in a stable and flexible chain consisting of 16 particles. These correlations can be found in the off-diagonal elements of the diffusion tensor which describe the correlations between an internal angle (α_i) in the chain with another (α_j). The diffusion tensor and how it is calculated will be described in more detail in section 2.2.2. The cross-correlations between angles can either be zero, positive or negative. These indicate that the angles are, respectively, 1) uncorrelated; when a change in α_i has no effect on α_j, 2) positively correlated; when an increase in α_i induces an increase in α_j, or 3) negatively correlated; when an increase in α_i induces a decrease in α_j.

We plotted the correlations between all joints α_i and α_j against the distance $\mid i - j \mid$ between the joints, averaging all correlations between joints at the same distance. The resulting graph and how the joints (α_i and α_j) and distance between those are defined are shown in Figure 1.18, in which γ_{ij} is the value of the correlation element between α_i and α_j in rad^{2}s^{-1}. When $i = j$ then $\mid i - j \mid = 0$ and the correlation value is simply the flexibility of that particular joint. As the graph contains the average correlation values, the point at $\mid i - j \mid = 0$ is the average flexibility of all bonds in the chain. Therefore, the graph is strongly positive when the distance between the bond is 0. The point at $\mid i - j \mid = 1$ is negative, demonstrating that bonds that are directly next to each other are negatively correlated. When the distance $\mid i - j \mid > 1$ the correlations decrease to 0, showing that bonds that are farther away from each other have little to no influence on each other.

There are two possible causes for the negative correlation between joints directly next to each other (at $\mid i - j \mid = 1$). The first reason is that the particles are connected to each other through the DNA linkers. When only one of the particles in the chain moves, its movement will induce a change in the internal angle of which it is the center particle and an opposite change in those directly next to it because these angles share axes.

The second possibility is that there are hydrodynamic interactions between neighbouring particles. This could couple their movements and through that the changes in the joints that they are part of.

From the acquired data cannot be concluded which of these is the (greater) cause for the correlations between neighbouring internal angles.
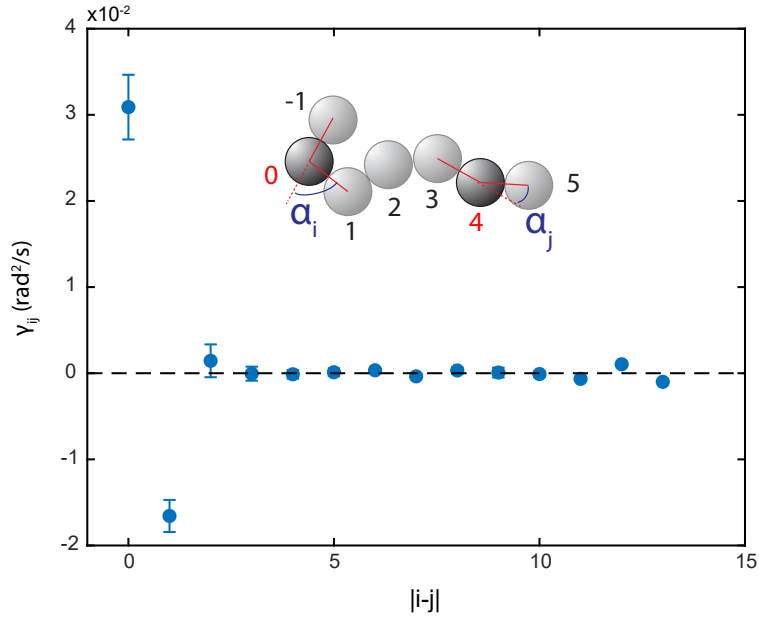
Figure 1.18: Graph showing the average correlations between bonds α_i and α_j as a function of distance $\mid i - j \mid$ between the bonds.

1.3.4   Chain relaxation

After removal of the magnetic field, the colloidal chains are free to move around and probe all possible conformations. As the chains are stretched out completely at t=0 after removal of the magnetic field, all other possible conformations are more compact than at t=0. The end-to-end distance ($R_{\text{end-end}}$, defined in Figure 1.19a) decreases through time as shown in Figure 1.19b. This graph shows the decrease in the average $R_{\text{end-end}}$ of three freely jointed chains, normalized against their initial $R_{\text{end-end}}$ at t=0. $R_{\text{end-end}}$ then varies around the mean-squared end-to-end distance $\langle R^2_{end-end} \rangle$.

   McMullen *et al.* found good agreement between measurements on their colloidomers made up of droplets and Flory theory for polymers. They measured the end-to-end distance ($\langle R^2_{end-end} \rangle$) for ≈ 2800 chains of two to twenty particles long and found that $\langle R^2_{end-end} \rangle \propto N^{0.72}$. Their results are shown in Figure 1.19c. For comparison, we did similar measurements on a smaller number of chains ranging from two to twenty-two particles long. Our results are shown in the same plot in Figure 1.19c. Both sets of data fit well with $\langle R^2_{end-end} \rangle = a N^{0.72}$, with different values of a due to a difference of about 0.7 μm in size of the monomers. Our measurements at $N = 16$ and $N = 21$ show a much higher $\langle R^2_{end-end} \rangle$ than expected from the fitted graph because the $\langle R^2_{end-end} \rangle$ value was determined too soon after removal of the magnetic field. The chains had not yet relaxed to their equilibrium $\langle R^2_{end-end} \rangle$.
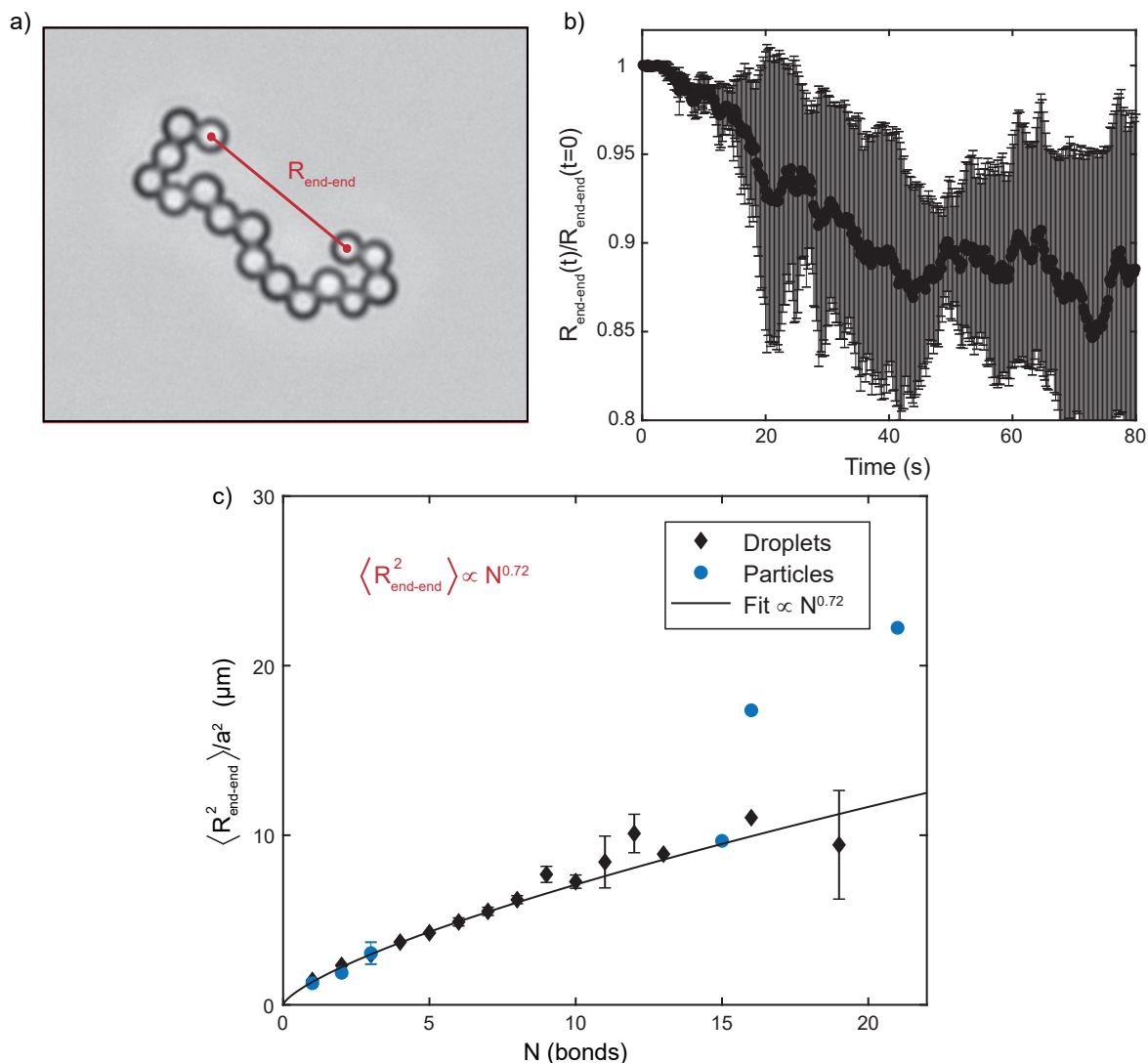
Figure 1.19: a) Schematic of how the end-to-end distance ($R_{\text{end-end}}$) is defined in a chain. b) Graph showing the decrease in average end-to-end distance of three chains against time. Adapted from [20]. c) Combination of data obtained on chains of droplets by [7] and chains of particles. The $\langle R^2_{end-end}\rangle/a^2$ as a function of the number of bonds in the chain.

1.4 Conclusions

In conclusion, we have succeeded in producing flexible trimers of SiO_2 particles of 2 μm in size. All internal angles could be probed at the same frequency, demonstrating that the bonds between the particles were freely jointed. The flexibility of the joints was determined from the initial slope of the mean-squared angular displacement against time. The produced trimers had a flexibility of 117.2 ± 26 deg^{2}s^{-1}, which is lower than was predicted from the flexibility of monomers in the samples. The decrease in flexibility is probably caused by drag of the DNA linkers in the lipid bilayer they are anchored in and the drag of the SiO_2 particles on each other.

The presence of an anti-sticking pHEA layer on the inside of the sample cell reduced the diffusion of all particles, the effect was found to be quite constant over all samples.

The storage time of samples outside the freezer did not influence the flexibility of the clusters.

According to [1] and [2] the largest influence on flexibility is would be the DNA linker density in the linker patch. However, the amount of linkers on each particle varied too much within a sample for us to exploit this dependence and tune the overall flexibility of clusters in a sample.

We observed a decrease in flexibility over a time of about 6 hours during which a freely jointed trimer stayed intact and flexible. The flexibility stabilized after these initial 6 hours and stayed stable for at least another 14 hours. The decrease in flexibility is most probably caused by accumulation of the DNA linkers to the bond area.[1] The minimum flexibility (and maximum patch size) is limited either by the amount of linkers on the surface of the length of the linkers.

Unbinding- and sticking events were observed in the system used in this project. The most probable cause for this is that the use of one type of DNA linkers with a self-complementary sticky end weakened the freely jointed bonds between the particles in comparison to systems wherein two different types of DNA linkers were used. It is not clear why this is the case.

In addition to clusters, long linear chains were produced by coating superparamagnetic particles with a layer of SiO_2 before adding the lipid bilayer and DNA linkers to the mix and letting the particles bind to each other in a magnetic field. However, not all particles formed bonds with their neighbours while being lined up in the magnetic field, limiting the length of the produced chains. This is most likely due to a deficiency of DNA linkers on their surface. The chains were also recorded to fall apart after various amounts of time, this is similar to the unbinding events that were noticed to happen in multiple flexible trimers. It is suspected that the unbinding events in the long chains were caused by the presence of pluronic F-127.[19] Analysis of the flexibility of the bonds in the chains showed two cases in which the chain broke at the most flexible bonds, giving the impression that the joints with the lowest amount of bound DNA linkers are the most fragile ones.

The flexibility in long chains was found to be influenced by the position of the bond. The joints were generally more flexible when they were situated closer to the edge of the chain. Flexibility decreases towards the middle of the chain.

The diffusion tensor of a flexible chain was used to investigate the correlations between different joints in a chain. It was found that neighbouring bonds correlated negatively with each other and that the correlation between bonds reduced rapidly to non-correlation as the distance between the bonds increased.

Finally, the end-to-end distance of several chains was measured through time. As the chains are produced by lining the particles up in a field, the end-to-end distance was always greatest at the start of measurement and decreased after removal of the field and allowing the chains to relax. The $\langle R^2_{end-end} \rangle$ of chains of several lengths was determined and compared to the trend described by McMullen *et al.* in [7]. According to [7], $\langle R^2_{end-end} \rangle \propto N^{0.72}$. This agreed excellently with our acquired data as well.

1.5   Outlook

The main difficulty that was encountered in this project was the reproducibility of the experiments. Performance of the same protocol for the synthesis of flexible clusters resulted sometimes in many flexibly bound clusters and sometimes in only rigidly bound clusters. The reason for this is yet unclear. However, there are some alterations to the protocol that might be tried. Firstly, 1,2-dilauroyl-sn-glycero-3-phosphocholine (DLPC) could be used as main ingredient in the lipid bilayers instead of the currently used DOPC. Secondly, pluronic F-68 can be added to the sample in a concentration of 0.1 wt% to stabilize the particles. This worked nicely in producing freely jointed colloidal droplets in [7]. As pluronic F-68 has a similar structure as pluronic F-127, it should be investigated whether F-68 is also able to remove DNA linkers from lipid bilayers. Lastly, the epoxy glue that is currently used to produce and seal the visualization cells may be releasing free radicals into the solution, destroying the vesicles. Therefore, the cells could be made with a different type of glue.

As described in section 1.2.4, the flexibility of a freely jointed trimer decreases through time until it stabilizes around its final flexibility. It would be highly interesting to do some fluorescence measurements on the bonding areas of the particles during the first 15 hours of being bound. This would confirm whether the decrease in flexibility is caused by the accumulation of DNA linkers in the bonding area, as is suspected from [1].

To solve the breaking events in longer freely jointed chains, several factors could be varied. The first tactic would be to optimize the amount of DNA linkers that are added to the samples to ensure that all particles have enough linkers on their surface for a valency of two. And secondly, no pluronic F-127 should be added to the samples.[19] As pluronic F-68 worked nicely in [7], this might be a good replacement. And failing that, the whole experiment could be repeated without surfactants present.

Long and stable chains could be used as a model to study the relaxation of polymers or proteins in solution. And specifically the effect of placement of semi-flexible and rigid bonds in the chain on its relaxation rate. This is especially interesting to study as an analogue to protein folding because proteins have flexible as well as rigid regions.

2

Diffusion of freely jointed trimers

Introduction

Since the first studies of Albert Einstein[21, 22] and Jean Perrin[23] on Brownian motion, diffusion of colloidal spheres has been studied extensively. This has resulted in the establishment of a solid basis of knowledge about the diffusion of colloidal spheres. For example, we know that the diffusion of a colloidal sphere is a stochastic process and that the Stokes-Einstein equation (equation 1.4) can be used to predict how fast a colloidal sphere diffuses. An example of the Brownian trajectory of a colloidal sphere is shown in Figure 2.1a. Additionally, we can predict how fast a diffusing colloidal sphere rotates by calculating the rotational diffusion coefficient (D_R) with $D_R = \frac{k_B T}{8\pi \eta a^3}$.[18] The time it takes for a spherical colloid with a radius of 2 μm to diffuse across its own radius or to significantly change its orientation is about 0.2 s.[18]

More recent studies have shown that asymmetry in a colloid's shape can alter the particle's Brownian motion. Alterations in shape can induce a preference in direction in which the particle is diffusing or cause coupling between different modes of motion.[24–30] In the Brownian trajectories of ellipsoidal particles (as shown in Figure 2.1) can clearly be seen that that colloids with an ellipsoidal shape prefer to move along their long axis, rather than along their short axis.[24] This preference is caused by the particles experiencing less hydrodynamic drag during the diffusion along their long axis than along their short axis.[24, 31, 32] Ellipsoids also show a slight coupling between their translational and rotational diffusion.[24] This means that translation induces rotation and vice versa. This effect has also been observed in boomerangs[25–27], asymmetric clusters[28, 29] and helices[30].

Asymmetry in translational diffusion and coupling between translational and rotational diffusion are difficult to find in a colloid's trajectory. These features can be studied with higher accuracy and can be quantified by measuring the colloid's hydrodynamic friction tensor or its diffusion tensor.[28, 29, 31, 32] The friction tensor and diffusion tensor are matrices containing the the friction- or diffusion constants of the colloid in all its degrees of freedom. Both tensors have been measured for colloidal clusters with various shapes.[28, 29] Examples of such clusters include regular trimers (Figure 2.1c), regular tetramers (Figure 2.1d) and irregular trimers (Figure 2.1e). The regular trimers are made up of spherical colloids of one size. An irregular trimer is made up of spherical colloids which all have a different size. The hydrodynamic friction tensor was extracted from short-time correlation functions in their orientationally resolved Brownian trajectories and showed that the translational and rotational motion in the irregular trimers are coupled. And that translation and rotation remain uncoupled in the regularly shaped trimers and tetramers.

In this work, we have added an additional complexity to the shape of colloidal clusters by allowing them to change their conformation during their diffusion. We studied the effect of the constantly changing shape on the cluster's Brownian motion. This has been made possible by the development of freely jointed colloidal clusters by Van der Meulen *et al.*[1] and Chakraborty *et al.*[2] This project is focused on the most simple freely jointed clusters in which a conformational change is visible: the freely jointed trimer.

In this chapter, we will first discuss and compare the translational and rotational diffusion coefficients of freely jointed trimers to rigid trimers with various conformations. Next, we will explore hydrodynamic correlations between the degrees of freedom of freely jointed trimers in 2D.
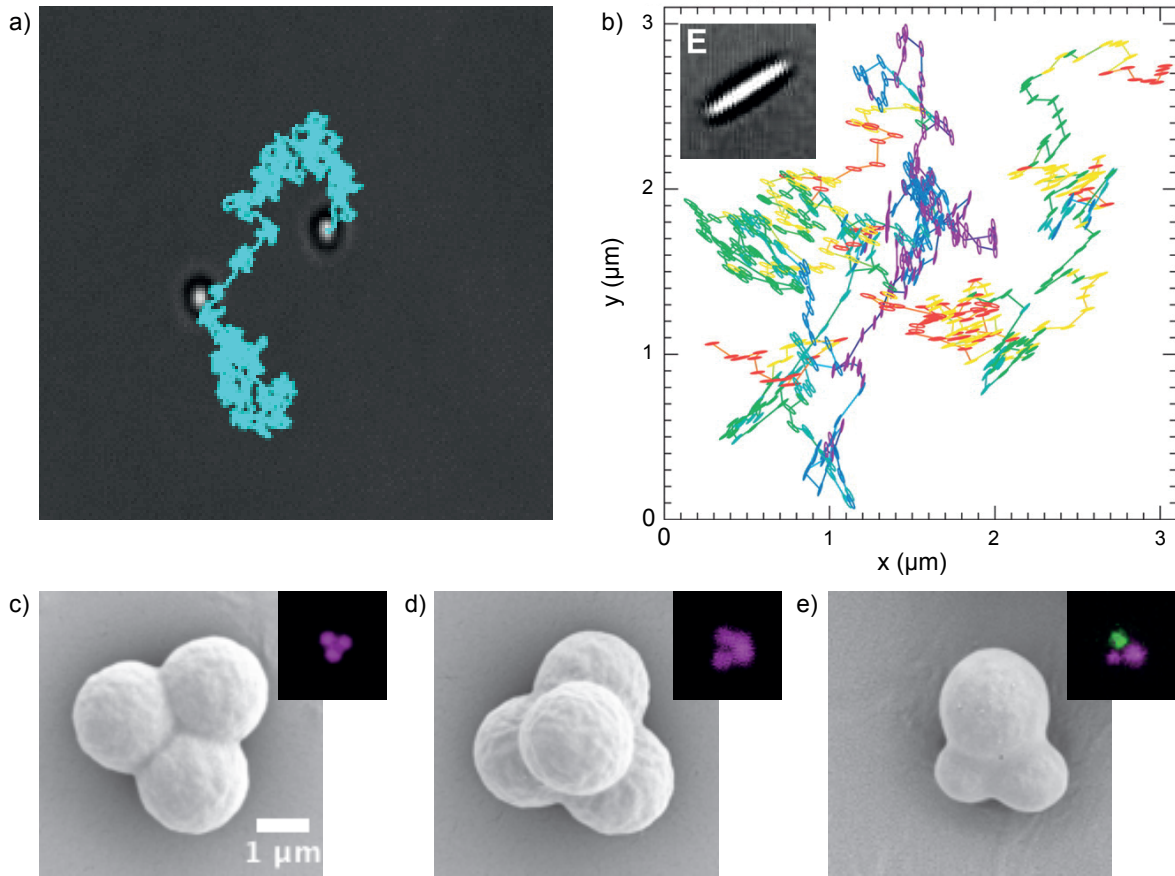

Figure 2.1: a) Random walk of a spherical colloid. b) Adapted from [24]. Random walk and orientations of an ellipsoid. The ellipsoids diffuses more in its elongated direction. c)-e) Adapted from [28]. Microscopy images of a regular trimer (c), regular tetramer (d) and an irregular trimer made up of spheres of three different sizes (e).

2.1 Methods

freely jointed trimers were produced, visualized and analyzed as described in section 1.1. Not all clusters in the samples were flexible, the samples always contained some rigidly bound clusters. To find differences in the diffusion of flexible and rigid trimers, 18 linear rigid trimers with different conformations were filmed, tracked and analyzed in the same way as the freely jointed trimers.

2.2 Results and Discussion

To find what the influence of a changing shape is on a colloid's Brownian motion, we studied and compared the translational and rotational diffusion of both rigid and freely jointed trimers. In this section, we first discuss the influence of shape shifting on translational and rotational diffusion. Later in this section, we discuss the effect of flexibility on hydrodynamic correlations within colloidal trimers.

2.2.1 Translational and rotational diffusion

In this section, we compare the translational and rotational diffusion coefficients of rigid and freely jointed trimers.

Prediction of D_T of rigid trimers

As mentioned before, the diffusion of a colloidal cluster is influenced by its shape. When considering a rigid cluster diffusing in 2D, its translational diffusion coefficient (D_T) can be split into the diffusion coefficients in the cluster's x-direction (D_{xx}) and its y-direction (D_{yy}). D_{xx} then tells us how fast the cluster diffuses parallel to its long axis and D_{yy} tells us how fast the cluster diffuses perpendicular to its long axis. The radius (a) in the Stokes-Einstein equation (equation 1.4) can then be replaced by the effective radius (a_{eff}) of the cluster perpendicular to the direction it is moving in. For colloidal trimers, a_{eff} is dependent on their conformation and thus on the internal bond angle α. For any conformation, we estimate D_{xx} and D_{yy} for rigid trimers through equations 2.1 and 2.2.

$$D_{xx} = \frac{k_B T}{6\pi\eta a_{eff,x}} \quad ; \quad a_{eff,x} = d \times \frac{1}{2}(cos(\frac{\pi - \alpha}{2}) + 1) \tag{2.1}$$

$$D_{yy} = \frac{k_B T}{6\pi\eta a_{eff,y}} \quad ; \quad a_{eff,y} = d \times \frac{1}{2}(2sin(\frac{\pi - \alpha}{2}) + 1) \tag{2.2}$$

with d the diameter of a monomer, k_B the Boltzmann-constant, T the temperature in Kelvin and η the viscosity of the medium in Pa·s.

Similarly, the rotational diffusion coefficient (D_R) can be predicted with equation 2.3. In which a_{eff} is the radius of the smallest sphere that fits around the whole cluster.

$$D_R = \frac{k_B T}{8\pi\eta a_{eff}^3} \quad ; \quad a_{eff} = d \times \frac{1}{2}(2sin(\frac{\pi - \alpha}{2}) + 1) \tag{2.3}$$

Equations 2.1, 2.2 and 2.3 were used to predict the translational diffusion coefficients in the x- and y-direction and the rotational diffusion coefficients of rigid trimers in all possible conformations. To better compare the predictions with experimental data, the measured translational diffusion coefficients of monomers used in Figure 1.9 were used to determine the influence of the pHEA layer on the viscosity in our samples. This resulted in an effective η of 2.443 mPa·s. The predicted values for D_{xx} and D_{yy} are shown in Figure 2.2.

Experimentally determined D_T and D_R

The the translational and rotational diffusion constants of 18 rigid trimers in different conformations were measured over a timescale of 6 seconds. The data were split into 5 bins according to the bond angle of the clusters. The average bond angles of the clusters in the resulting bins were plotted against the average D_{xx}, D_{yy} and D_R. These results are shown in Figure 2.2. The data points contain, from left to right, one, four, six, two and four clusters, respectively.

The predicted and experimental data on rigid trimers in Figure 2.2a show the same trend. The diffusion in the x-direction is at its maximum when the shape of the cluster resembles that of a rod ($\alpha = 0^o$) and decreases as the cluster folds up to form its most compact triangular like form ($\alpha = 120^o$). The opposite is observed for the diffusion in the y-direction, which is at its minimum at $\alpha = 0^o$ and at its maximum at $\alpha = 120^o$. The predicted and the experimental values of D_{xx} and D_{yy} approach each other at similar values for D_{xx} and D_{yy} at $\alpha = 120^o$. The difference in D_{xx} and D_{yy} at $\alpha = 0^o$ is larger in the predicted than in the experimental data.

The D_{xx} and D_{yy} of freely jointed trimers were measured over the same timescale as for the rigid trimers. These are also plotted in Figure 2.2a and represented as horizontal lines. We had expected that these values would be similar to the weighted average of D_{xx} and D_{yy} of the conformations of the rigid trimers that are shown in the same figure. However, this is not what we measured. The measured values of D_{xx} and D_{yy} of freely jointed trimers are lower than those measured for the rigid trimers in their various conformations. This reveals that flexible trimers systematically show slower translational diffusion than their rigid counterparts.

The trends of the predicted and experimentally determined D_R values in Figure 2.2b are in agreement as well. Both curves show that rigidly bound rod-like clusters rotate slower than triangular clusters. The experimentally determined curve lies at much higher values and increases more sharply than the predicted curve. We suspect that this difference is caused by the assumptions that were made in the predictions. We chose a_{eff} as the radius of the smallest sphere that fits around the whole cluster. Such a sphere has a significantly larger volume than the actual cluster and the shape of the cluster does not resemble a sphere in any of its conformations. Similarly to the translational diffusion coefficients, the average D_R of flexible trimers was expected to be a weighted average of the rotational diffusion coefficients of all conformations of the rigid trimers. However, the measured rotational diffusion of the flexible trimers was as low as the D_R of the slowest rotating rigid clusters.

Therefore, we suspect that freely jointed bonds slow down the diffusion of the colloidal clusters, resulting in slower translational and rotational diffusion as compared to rigidly bound colloidal clusters.
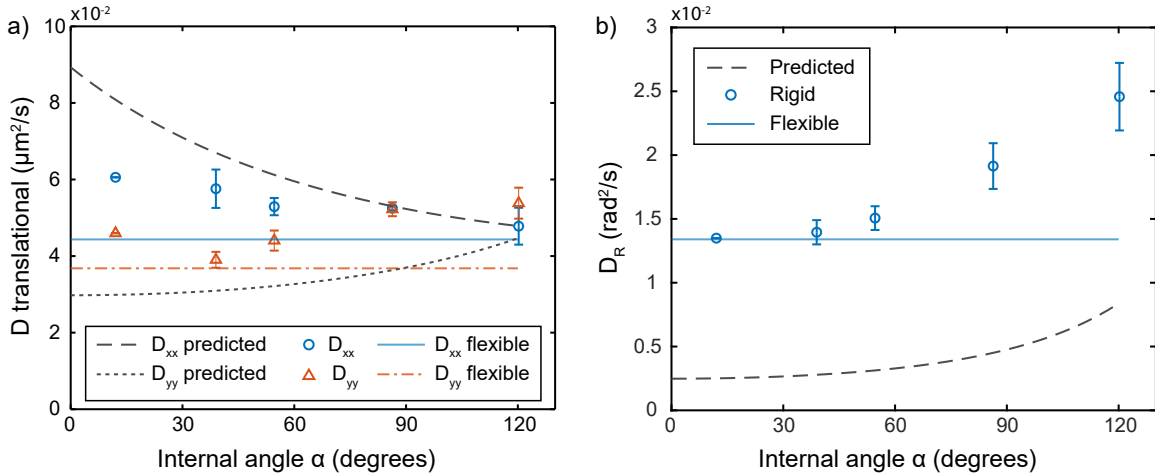
Figure 2.2: Comparison between diffusion of rigid and freely jointed trimers. a) Translational diffusion coefficients of the clusters in the x- (D_{xx}) and y-direction (D_{yy}), predicted and measured values are shown. Both coefficients are also shown for flexible trimers. b) Predicted and measured rotational diffusion coefficient of rigid trimers and the average rotational diffusion coefficient of flexible trimers.

To examine the difference in translational and rotational diffusion between rigid and freely jointed trimers shown in Figure 2.2 more thoroughly, a histogram of all diffusion coefficients of all rigid and flexible trimers is shown in Figure 2.3. Figure 2.3a shows all measured translational diffusion coefficients (D_T) and Figure 2.3b shows all measured values of D_R. These histograms shows that the flexible and rigid trimers form two different populations in both D_T and D_R, with the lower values belonging to the flexible trimers. There is some overlap between the populations in both histograms. Nevertheless, these results support the hypothesis that introducing freely jointed bonds slows down the diffusion of a cluster.

freely jointed dimers

The finding that freely jointed trimers have lower translational and rotational diffusion constants than rigid trimers of any shape has an interesting consequence for the identification of flexible dimers. Contrary to the situation for trimers, the change in bond angle cannot be directly seen in two-particle clusters. In dimers, it is impossible to distinguished a rotation of the whole cluster from a change in bond angle by simply looking at the cluster. This makes it seemingly impossible to find out whether a dimer is connected through a rigid or a freely jointed bond. However, our finding on dependence of D_T and D_R on bond flexibility suggests that we could distinguish between rigid and flexible dimers by measuring their translational and rotational diffusion.

To test this hypothesis we measured the the translational and rotational diffusion of dimers in our samples. We tracked 9 dimers in our samples and split all movies per 200 frames (40 seconds). We determined D_T and D_R in each set of 200 frames on a timescale of 0.4 s. Histograms of the obtained D_T and D_R values are shown in Figures 2.3c and Figure 2.3d, respectively. Figure 2.3d very clearly shows two populations with no overlap between them, therefore the D_R of all dimers were used to divide them into two groups. We assumed that the population with high D_R (> 1.5) are rigidly bound dimers and the population with lower D_R (< 1.5) are freely jointed dimers. The dimers in Figure 2.3c

were split into two groups accordingly. This also resulted in two populations, showing that the dimers with low D_R are the same dimers as those with low D_T, although with some overlap between the two.

With this experiment, we have showed that there are two populations of dimers present in our samples. One population with high D_T and D_R and one population with lower D_T and D_R coefficients. We suspect that the population with higher diffusion constants (population 2 in Figures 2.3c-d) consists of rigid dimers and that the population with lower diffusion constants (population 1 in Figures 2.3c-d) consists of freely jointed dimers.

Additional experiments should be performed to check whether these populations are truly a rigid and a flexible population.
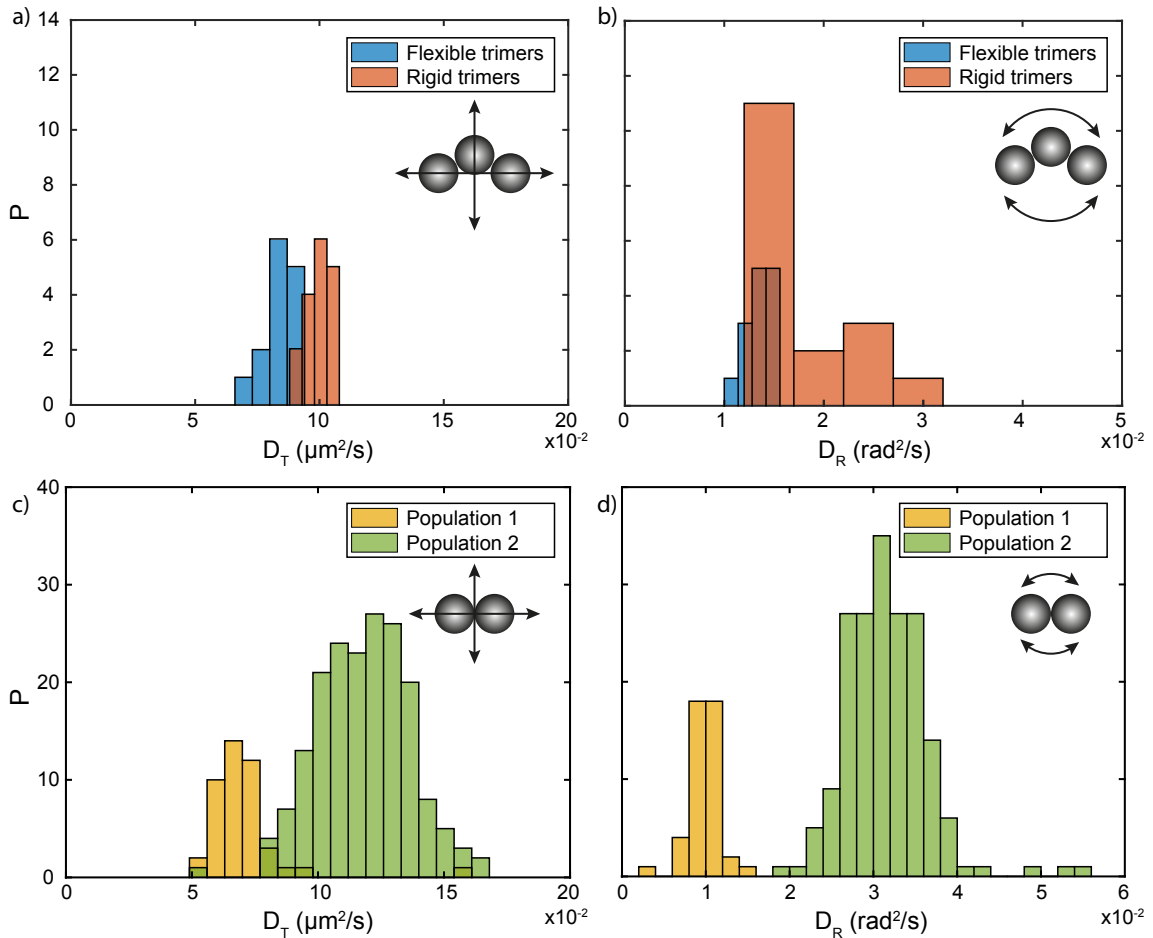

Figure 2.3: a) Histogram of the measured D_T values of the analyzed flexible and rigid trimers. b) Histogram of the measured D_R values of the analyzed flexible and rigid trimers. c) Populations were determined using the data in histogram d. All particles with $D_R < 1.5$ were labeled as flexible and grouped accordingly. d) Histogram of the measured D_R of all dimers. The dimers in the population with lower D_T were assumed to be flexible and those with higher D_T were assumed to be rigidly bound.

Cause of low D_T in flexible trimers

That the diffusion of a freely jointed cluster is slower than the diffusion of a rigid cluster can be understood by considering the diffusion of the center of mass of a rigid cluster consisting of three particles, and the combined center of mass of three particles in solution that are not attached to each other. Schematic representations of these two situations are shown in Figures 2.4a and 2.4b. The combined center of mass of the three particles in both situations are indicated with a blue dot in figures a and b. The center of mass of the clustered particles in situation a) is influenced differently by the Brownian motion of the cluster than by the Brownian motion of the unattached particles in situation b). In situation a), the three particles can only move as a whole, because their positions are fixed relative to each other. Therefore, when one particle moves (indicated with the red arrow), the other two move with it and so does their combined center of mass (indicated with the blue arrow). While in situation b), the particles move independently, with no influence on each other whatsoever. Therefore, only a subsection of all displacements of the individual particles leads to the displacement of the cluster's center of mass. For example, when all three particles move directly away from the center of mass, as indicated with red arrows in Figure 2.4b, their center of mass stays fixed in the same position even though all particles have changed their positions. When the diffusion of the centers of mass in situations a) and b) would be tracked and analyzed, the center of mass in situation a) would have a higher translational diffusion coefficient than in situation b), as it will move more often.

The situation for a freely jointed trimer is not equal to the one sketched for unattached particles. It is rather a situation in between a rigid cluster and three independent particles. Considering a freely jointed trimer as such explains why the diffusion of freely jointed clusters is slow compared to their rigid counterparts.
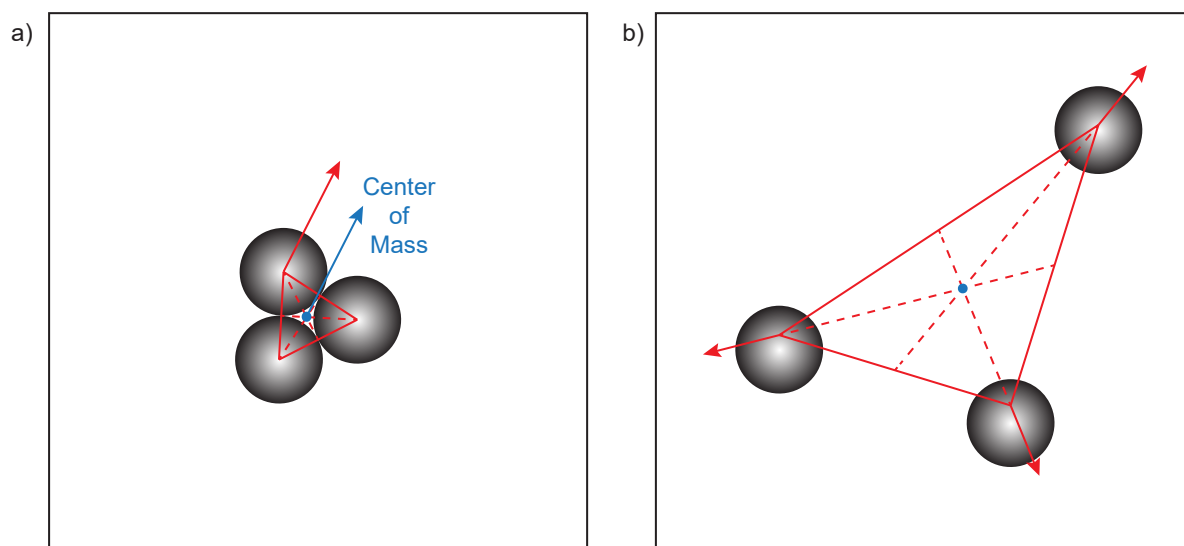

Figure 2.4: Schematic representation of the movement of the center of mass (indicated by the blue dot) of three particles, as a result of movement of particles (indicated with red arrows) when the particles are a) attached to each other or b) moving independently from each other. In a), the center of mass will move with every movement of any of the three particles forming the cluster. In b), not all movement of the particles results in displacement of the center of mass, for example when all particles move the same distance directly outwards.

2.2.2 Hydrodynamic correlations

In this section, we first discuss how hydrodynamic correlations between translation, rotation and changes in conformation can be analyzed by measuring the diffusion tensor of the particle in question. We then show the diffusion tensors we measured for rigid and freely jointed trimers diffusing in two dimensions and compare these to find the effect of a changing bond angle on hydrodynamic correlations within a colloidal trimers. We expect to see no coupling between translation, rotation and conformation in rigid clusters. We we do expect to see coupling between translation and conformational changes in freely jointed clusters because this is also observed in macroscopic objects, such as a swimming squid. This will be explained in more detail later in this section.

Diffusion tensor

Coupling between time-dependent variables, of a cluster can be studied through correlation functions and the diffusion tensor of the cluster. We will first discuss which degrees of freedom rigid and freely jointed clusters have when diffusing in two dimensions. Next, we discuss how correlation functions between the degrees of freedom can be calculated. Lastly, we discuss how the diffusion tensor can be extracted from the correlation functions and how the diffusion tensor can be used to determine which degrees of freedom are coupled.

   A rigid cluster moving in two dimensions has three degrees of freedom; translation in the x-direction, translation in the y-direction and rotation. When the cluster is not rigid, but flexible, the cluster's conformation can also change through time and is added as a fourth degree of freedom. Our purpose is to find correlations between these time-dependent variables. Figure 2.5a shows a schematic representation of how the orientation (θ), lab- and body frame of a cluster are defined. In which the lab frame is the frame of the camera in the microscope, with x_{lab} on the horizontal axis and y_{lab} on the vertical axis. The x-axis of the body frame is defined as the axis connecting the centers of the two edge particles. The y-axis is the axis perpendicular to this, through the center of the middle particle. The direction of the y-axis that points to the middle particle is considered positive. The orientation of the particle is defined as the angle θ between the x-axes of the lab- and the body frame. The conformation of the particle is determined by the internal angle α, which is the angle between the extension of the line connecting the centers of particles 1 and 2 and the line connecting the centers of particles 2 and 3, which is shown in Figure 2.5b.

   When x, y, θ and α are known at all times t, the correlation functions between all four variables can be calculated. The correlation functions between two time-dependent variables V and W are defined as equation 2.4. Calculations of all combinations of variables results in $4 \times 4 = 16$ functions, of which six sets of two are equal. The slopes of the correlation functions in small time intervals can be calculated through equation 2.5.[28]

$$C_{VW}(\delta t) = \langle (V(t + \delta t) - V(t))(W(t + \delta t) - W(t)) \rangle_t \tag{2.4}$$

$$D_{VW} = \frac{1}{2} \lim_{\delta t \to 0} \frac{\partial C_{VW}(\delta t)}{\partial \delta t} \tag{2.5}$$

The slopes of the correlation functions can be collected in a new 4×4 matrix. This matrix is called the diffusion tensor. The elements of the diffusion tensor indicate the correlation
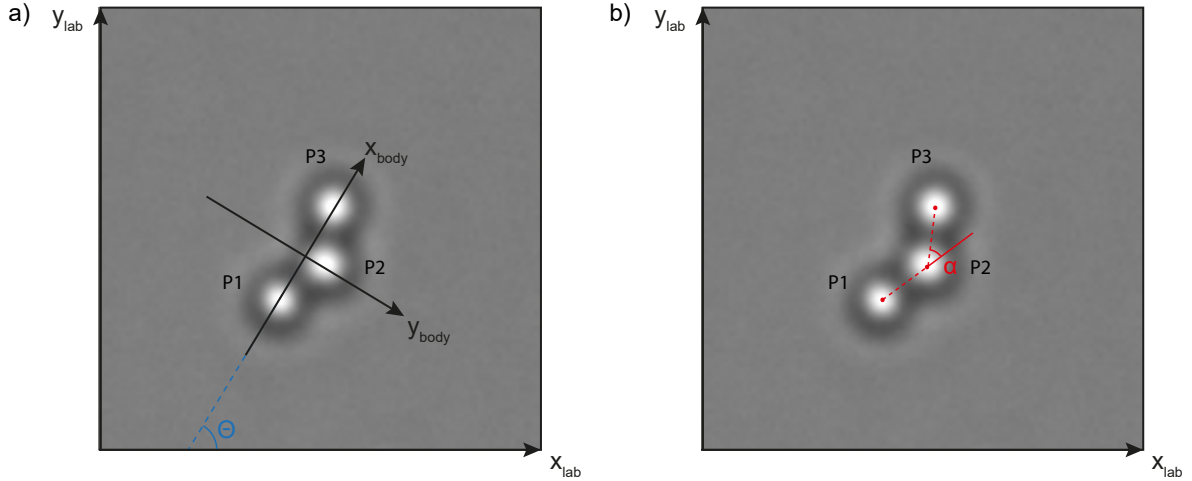
Figure 2.5: Schematic representation of how the θ, lab- and body frame (a) and the internal angle α (b) are defined.

between the two variables their correlation function contains. Positive elements indicate a positive correlation between the particular degrees of freedom. Positive correlation means that when one variable increases the other increases as well, and when one decreases, the other decreases as well. Negative elements indicate anti-correlation. This means that when one variable increases, the other decreases and vice versa. Elements that are equal to zero indicate non-correlation, meaning that the variables are not coupled.

Hydrodynamic correlations in rigid clusters

As mentioned above, a rigid cluster that is confined to two dimension has three degrees of freedom; its position in x and y and its orientation. Its conformation is fixed and thus not time-dependent. Calculating the hydrodynamic correlation functions between these degrees of freedom yields a 3×3 matrix. The on-diagonal elements of this matrix are the correlation of the degrees of freedom with themselves, which is equal to their variance. These are thus the diffusion coefficients in the x- and y-directions and the diffusion coefficient in θ, the rotational diffusion coefficient of the cluster (D^R). Cross-correlations are only expected to be found in asymmetrical particles. The rigid clusters in this project are always symmetrical in the y_{body}-axes, so we expect to find no cross-correlations. In the diffusion tensor this translates into off-diagonal elements that are equal to zero. Therefore, the diffusion tensor that we expect to measure for our rigid particles is

$$ D = \begin{bmatrix} D_{xx} & 0 & 0 \\ . & D_{yy} & 0 \\ . & . & D_{\theta\theta} \end{bmatrix} \quad \text{or} \quad D = \begin{bmatrix} D_{xx} & 0 & 0 & 0 \\ . & D_{yy} & 0 & 0 \\ . & . & D_{\theta\theta} & 0 \\ . & . & . & D_{\alpha\alpha} = 0 \end{bmatrix} $$

when the internal angle is also considered. Because the internal angle is not time-dependent in a rigid cluster, no correlations with D_α should exist. The dots indicate mirror symmetry in the diagonal. The unit of the elements containing only D_x and D_y is $\mu m^2 s^{-1}$, the elements containing only D_θ and D_α is $rad^2 s^{-1}$ and the unit of those containing a combination of D_x or D_y and D_θ or D_α is $\mu m \cdot rad \cdot s^{-1}$.

We calculated the correlation functions of the rigid particles that were discussed in section 2.2.1 and determined the slope of the function between the first two points, this corresponds to a Δt of 0.2 s. This resulted in the following diffusion tensor

$$D = 10^{-2} \times \begin{bmatrix} 4.12 \pm 0.23 & -0.02 \pm 0.05 & 0.02 \pm 0.12 & 0.00 \pm 0.03 \\ . & 3.75 \pm 0.31 & 0.01 \pm 0.05 & -0.05 \pm 0.05 \\ . & . & 1.40 \pm 0.39 & 0.00 \pm 0.02 \\ . & . & . & 0.26 \pm 0.15 \end{bmatrix}$$

Which shows clearly positive values for D_{xx}, D_{yy} and $D_{\theta\theta}$. The tensor shows that $D_{xx}{>}D_{yy}$, as is expected as the length of the clusters is always greater than the height. Therefore, the diffusion in the y-direction of the cluster is always submitted to more drag of the solvent. Although expected to be zero for rigid trimers, $D_{\alpha\alpha}$ is slightly positive. This indicates that not all trimers that are included in the averaged tensor were found to be perfectly rigid. This can be caused either by an inaccuracy in the tracking procedure or by a very slight flexibility in the bonds. This is possible because they were also coated with lipids and DNA-linkers. However, they were not visibly flexible in the recorded movies. Even though it is slightly positive, the measured $D_{\alpha\alpha}$ is a factor 18 lower than what we find in the clusters that we considered as freely jointed (see section 2.2.2).

All off-diagonal elements are close to zero and not significantly positive or negative. Only $D_{y\alpha}$ is slightly negative. This can be connected to the slight flexibility that we measured in the clusters and will be discussed in more detail in section 2.2.2. This element is expected to be closer to zero when the clusters are perfectly rigid. Therefore, the same measurements should be performed on aggregated particles without lipid bilayer and DNA-linkers on their surface. This would eliminate all chance of forming freely jointed bonds. If this does not result in a $D_{y\alpha}$ that is closer to zero, the accuracy in the tracking procedure should be improved.

Hydrodynamic correlations in freely jointed clusters

When a flexible internal angle is introduced, α becomes time-dependent as well. Then, the on-diagonal element $D_{\alpha\alpha} > 0$, as $D_{\alpha\alpha}$ is the variance of the internal angle and the angle is now free to change during diffusion. $D_{\alpha\alpha}$ can be used as a measure for the flexibility of the bond. How this additional (internal) degree of freedom correlates with x, y and θ during diffusion will be explored in this section.

$$D = \begin{bmatrix} D_{xx} & 0 & 0 & ? \\ . & D_{yy} & 0 & ? \\ . & . & D_{\theta\theta} & ? \\ . & . & . & D_{\alpha\alpha} \end{bmatrix}$$

Figure 2.6a shows a trimer with the +y, -y and α indicated. The internal angle α is negative in this picture because it points down from the extended line between particles 1 and 2. When the cluster moves in the +y direction and the resistance of the solvent on the outer particles exerts a force that is larger than the resistance of the DNA-linkers in the lipid bilayers on the particles, the outer particles will be pushed downwards. This would make α more negative by an amount of $-\delta\alpha$. This effect has been illustrated in Figure 2.6b. When the cluster moves downwards (-y), the effect is reversed (as illustrated in Figure 2.6c). The resistance of the solvent is then directed upwards and thus pushes the outer particles upwards with it. This would make increase

α by an amount of $+\delta\alpha$. Therefore, when the y-coordinate of the position of the center of mass increases, α decreases. And when the y-coordinate of the center of mass decreases, α increases.[1] Therefore, we expect to see a negative correlation between y and α ($D_{y\alpha}$) in the diffusion tensor, giving us

$$D = \begin{bmatrix} D_{xx} & 0 & 0 & 0 \\ \cdot & D_{yy} & 0 & -\delta \\ \cdot & \cdot & D_{\theta\theta} & 0 \\ \cdot & \cdot & \cdot & D_{\alpha\alpha} \end{bmatrix}$$
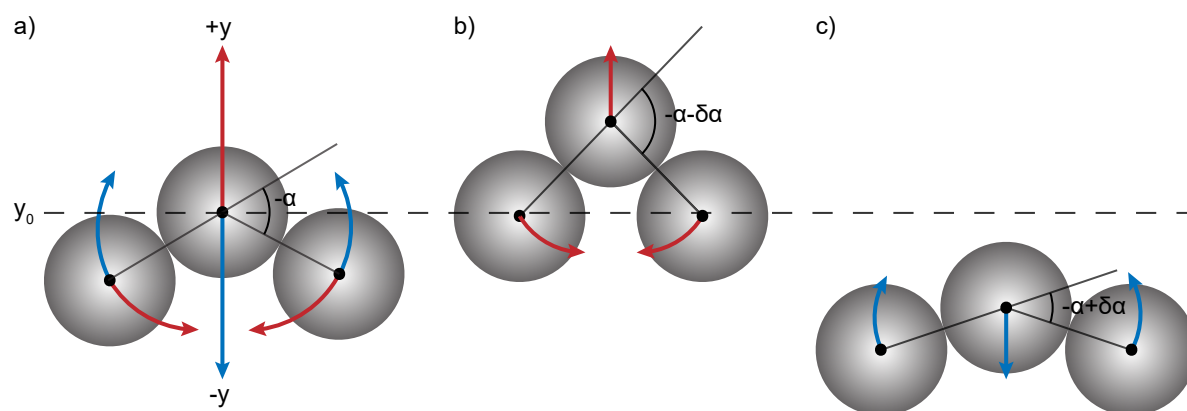
Figure 2.6: Expected correlation between diffusion of the cluster in the y-direction and the internal angle α.

Six freely jointed trimers that were fairly isolated from other particles in the sample were tracked and their correlation functions were calculated using equation 2.4 and averaged. This resulted in the correlation functions in Figure 2.7. These graphs seem to agree with our expectations. The functions on the diagonal all have a clearly positive slope, while the off-diagonal graphs are practically horizontal. Only the graph at Yα has a negative slope.

Equation 2.5 was used to calculate their slopes at a timescale of 0.2 s and the elements of the averaged diffusion tensor. This gave the following diffusion tensor for the freely jointed trimers

$$D = 10^{-2} \times \begin{bmatrix} 5.46 \pm 0.30 & -0.02 \pm 0.10 & 0.00 \pm 0.16 & 0.00 \pm 0.10 \\ \cdot & 4.21 \pm 0.21 & 0.02 \pm 0.03 & -0.60 \pm 0.08 \\ \cdot & \cdot & 1.53 \pm 0.14 & 0.02 \pm 0.21 \\ \cdot & \cdot & \cdot & 4.61 \pm 0.10 \end{bmatrix}$$

This tensor indeed shows clearly positive on-diagonal elements and off-diagonal elements that are zero within their standard deviation. $D_{y\alpha}$ is the only off-diagonal element that is clearly non-zero. It is also negative, showing the negative correlation between y and α that was expected to be present in freely jointed trimers. The value for $D_{y\alpha}$ in this tensor is a factor 12 more negative than the $D_{y\alpha}$ that was measured in rigid trimers. Therefore,

---

[1]One can imagine the flexible trimer as a squid swimming up by pushing its tentacles down and swimming down by pushing its tentacles back up. This is nicely illustrated at `https://gfycat.com/serpentinewidegoitered`.
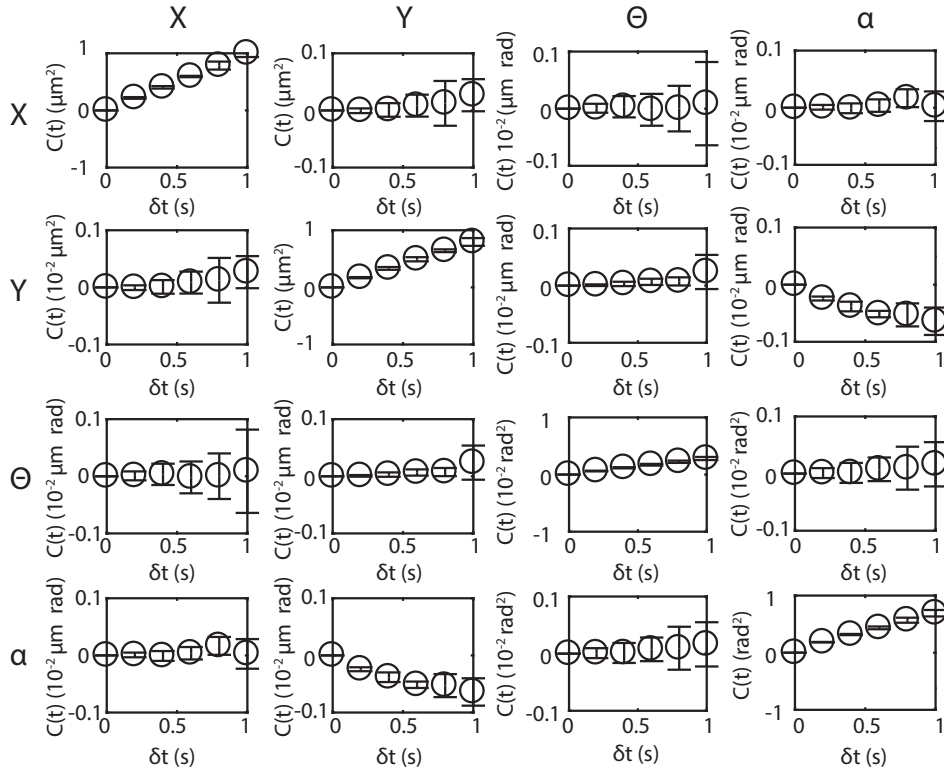
Figure 2.7: Measured hydrodynamic correlation functions, averaged for 6 flexible trimers.

we suspect that this correlation is genuinely caused by the flexibility of the bonds and not by an artefact in the tracking procedure.

The diffusion tensor also shows nicely that the freely jointed trimers diffuse more in their x-direction than in their y-direction due to larger resistance of the solvent on the larger width of the clusters.

Sensitivity of $D_{y\alpha}$

To our surprise, we measured a slightly negative correlation between y and α in trimers that were not visibly flexible. We suspected that this correlation was caused by a very slight bond flexibility. To explore this concept further, the diffusion tensors of all tracked trimers were calculated at a timescale of 0.2 s. The trend between the $D_{\alpha\alpha}$ (flexibility J) and $D_{y\alpha}$ elements in the resulting diffusion tensors is shown in Figure 2.8. The measured bond flexibilities of the particles that were considered rigid and for which a negative average $D_{y\alpha}$ was measured, were in the range between 4 deg^2s^{-1} and 24 deg^2s^{-1}. Figure 2.8 shows that the correlation $D_{y\alpha}$ is indeed stronger for clusters with a higher flexibility, even at the low flexibilities measured in the rigid particles. This finding is consistent with our hypothesis that the negative average correlation in $D_{y\alpha}$ is caused by slight flexibility of the bonds.

The trend continues in trimers with higher flexibility between 120 deg^2s^{-1} and 170 deg^2s^{-1}, showing that the measured correlation between D_y and D_α is stronger in freely jointed trimers with higher bond flexibility. This trend is not surprising because a more flexible bond is expected to require less force to change. Therefore, the drag caused by a translation of the same magnitude can result in a larger change in bond angle. This would give a stronger correlation between the translation in y-direction and the change

in the internal bond angle α.

Even though these results make it plausible that the negative correlation in $D_{y\alpha}$ was caused by the slight flexibility of the bonds, truly rigid trimers should be made to confirm that it was not caused by a tracking artefact. This could be done by using the same method for coating the SiO_2 particles with a lipid bilayer to keep the experimental conditions as close to those the freely jointed trimers are measured in, without adding the DNA linkers. This way we can ensure that all clustered particles are joined by a rigid bond. For completely rigid clusters, the measured correlation in $D_{y\alpha}$ should be zero.
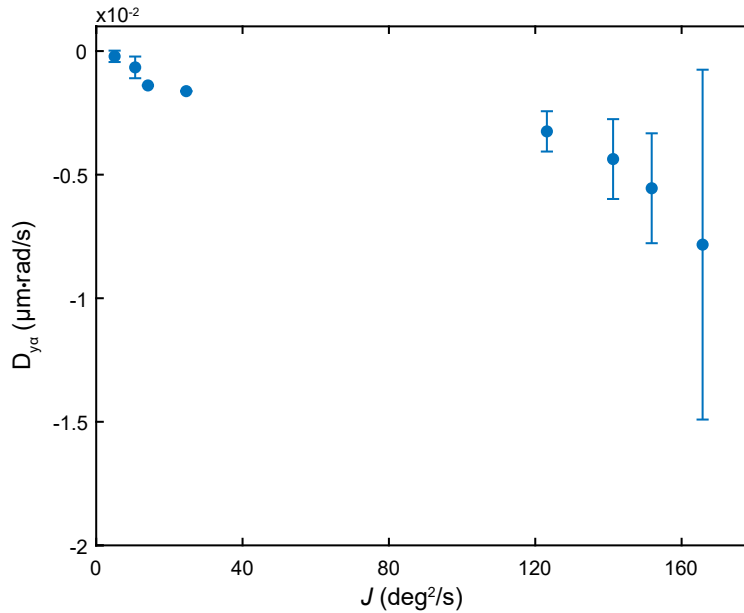

Figure 2.8: The correlation between the translation in the y-direction and the changing internal angle α as a function of joint flexibility.

2.3 Conclusions

We studied the Brownian motion of rigid and freely jointed colloidal trimers to investigate the effect of a changing shape on the diffusion of colloidal objects. We found two main differences in the diffusional behaviour of the freely jointed and rigid clusters.

The first difference that we found was that both translational and rotational diffusion are slower in freely jointed trimeric clusters than their rigid counterparts. This slowing of the diffusion is due to the particles within the cluster moving more independently than when they are rigidly bound. This results in less displacements of the center of mass because not all movements of the particles result in a displacement of the center of mass.

To test whether this finding could be used to distinguish between rigid and flexible dimers, the translational and rotational diffusion coefficients of dimers in the samples were measured as well. We found that there are indeed two populations of dimers in our samples, one with high translational and rotational diffusion constants and one with low translational and rotational diffusion constants. We hypothesize that the population that has high diffusion constants consists of rigidly bound dimers and that the population with lower diffusion constants consists of freely jointed dimers.

The second difference that we found lies in the correlations between the degrees of freedom. These could be quantified by measuring the correlation functions of several

rigid and freely jointed clusters over time and determining the initial slopes to calculate the corresponding diffusion tensors. As expected, the rigid clusters showed no significant cross-correlations between D_x, D_y, D_R and D_α. The averaged diffusion tensor of the rigid clusters did have a slightly negative correlation between the diffusion in the cluster's y-direction and the changing internal angle α. We suspect that this correlation was caused by a slight flexibility of some of the clusters that were considered as rigid. A much stronger correlation $D_{y\alpha}$ was found for the freely jointed clusters. This shows that at short timescales, α decreases when the cluster moves in its positive y-direction and vice versa.

2.4   Outlook

More experiments have to be performed to confirm that the two populations of dimers with different diffusion constants that were present in our samples are indeed a population of rigid dimers and a population of freely jointed dimers. This could be done by applying optically visible markings on a spot on each monomer. A possible method to accomplish such a marking is by coating colloidal particles with a fluorescent silica layer and using a laser to bleach a spot on the colloid, either prior to or after coating with a lipid bilayer. However, care should be taken that the lipid bilayer is not destroyed by the laser. If the bleached spots on two bound monomers move in respect to each other, the monomers are expected be joined by a freely jointed bond. If the markers do not move in respect to each other, the dimer is expected to be rigidly bound. This experiment can be performed on trimers as well to check whether these expectations are accurate.

A more simple experiment to find the average D_T and D_R of rigid dimers is to measure these constants in dimers coated only with lipids. This way, there is no possibility of establishing a freely jointed bond, due to the absence of DNA linkers. Therefore, all produced dimers will be rigidly bound. Next, the measured diffusion coefficients can be compared to those of the two populations of dimers coated with both a lipid bilayer and DNA linkers.

This last experiment can also be used to measure the diffusion tensor of truly rigid trimers. This should result in a tensor with the elements $D_{\alpha\alpha}$ and $D_{y\alpha}$ both equal to zero, if the previously measured non-zero elements are not caused by an inaccuracy in the particle tracking procedure. This would allow us to better compare the hydrodynamic correlations in rigid and freely jointed trimers.

Lastly, it would be fascinating to measure hydrodynamic correlations in longer linear clusters and chains. Such clusters and chains could be produced with the method described in section 1.3, using paramagnetic SiO_2 particles. Hydrodynamic correlations within the clusters and chains can be measured in the same way as described in section 2.2.2. This could give insight into hydrodynamic correlations in polymers in solution.

Acknowledgements

Bibliography

[1]   Stef A.J. van der Meuler and Mirjam E. Leunissen. "Solid colloids with surface-mobile DNA linkers". In: *Journal of the American Chemical Society* 135.40 (2013), pp. 15129–15134.

[2]   Indrani Chakraborty et al. "Colloidal joints with designed motion range and tunable joint flexibility". In: *Nanoscale* 9 (23 2017), pp. 7814–7821.

[3]   Dave Gerr. *Propeller Handbook: the complete reference for choosing, installing and understanding boat propellers.* International Marine, 1989. ISBN: 0-07-138176-7.

[4]   Ayan Chakrabarty et al. "Brownian motion of boomerang colloidal particles". In: *Physical Review Letters* 111 (16 2013), pp. 160603–160608.

[5]   Julie Byrom et al. "Directing assembly of DNA-coated colloids with magnetic fields to generate rigid, semiflexible, and flexible chains". In: *Langmuir* 30.30 (2014), pp. 9045–9052.

[6]   Hanumantha Rao Vutukuri et al. "Colloidal analogues of charged and uncharged polymer chains with tunable stiffness". In: *Angewandte Chemie International Edition* 51.45 (2012), pp. 11249–11253.

[7]   Angus McMullen et al. "Colloidomers: freely jointed polymers made of droplets". In: *Physical Review Letters* 121 (13 2018), pp. 138002–138007.

[8]   Eric M. Furst et al. "Permanently linked monodisperse paramagnetic chains". In: *Langmuir* 14 (26 1998), pp. 7334–7336.

[9]   Sibani Lisa Biswal and Alice P. Gast. "Mechanics of semiflexible chains formed by poly(ethylene glycol)-linked paramagnetic particles". In: *Physical Review E* 68 (2 2003), p. 021402.

[10] Maik Hadorn et al. "Specific and reversible DNA-directed self-assembly of oil-in-water emulsion droplets". In: *Proceedings of the National Academy of Sciences* 109 (50 2012), pp. 20320–20325.

[11] Lang Feng et al. "Specificity, flexibility and valence of DNA bonds guide emulsion architecture". In: *Soft Matter* 9 (41 2013), pp. 9816–9823.

[12] Sonja I.R. Castillo. *Cubic Colloids: synthesis, functionalization and applications.* 2015. ISBN: 978-94-6108-870-3.

[13] V Prasad, D Semwogerere and Erik R. Weeks. "Confocal microscopy of colloids". In: *Journal of Physics: Condensed Matter* 19.11 (2007), p. 113102.

[14] Sigma-Aldrich. *Pure water density standard.* URL: https://www.sigmaaldrich.com/catalog/product/sial/denwat3?lang=en&region=NL. (accessed: 08.04.2019).

[15] Sigma-Aldrich. *Silicon dioxide.* URL: https://www.sigmaaldrich.com/catalog/product/aldrich/381268?lang=en&region=NL. (accessed: 08.04.2019).

[16] John C. Crocker and David G. Grier. "Methods of digital video microscopy for colloidal studies". In: *Journal of colloid and interface science* 179 (1 1996), pp. 298–310.

[17] Daniel T. Gillespie and Effronsyni Seitaridou. *Simple Brownian Diffusion: An introduction to the standard theoretical models.* Oxford University Press, 2013. ISBN: 978-0-19-966450-4.

[18] Albert P. Philipse. *Brownian Motion: Elements of colloid dynamics.* Undergraduate Lecture Notes in Physics. Springer International Publishing, 2018. ISBN: 978-3-319-98053-9.

[19] Melissa Rinaldin et al. "Colloid supported lipid bilayers for self-assembly". In: *Soft Matter* 15 (6 2019), pp. 1345–1360.

[20] Pepijn G. Moerman. *Dynamics of Active Droplets and Freely-Jointed Colloidal Trimers.* 2019. ISBN: 978-94-6380-337-3.

[21] Albert Einstein. "Über die von der molekularkinetischen Theorie der Warme geforderte Bewegung von in ruhenden Flussigkeiten suspendierten Teilchen". In: *Annalen der Physik* 322.8 (1905), pp. 549–560.

[22] Albert Einstein. "Eine neue Bestimmung der Moleküldimensionen". In: *Annalen der Physik* 324.2 (1906), pp. 289–306.

[23] Jean Perrin. "Mouvement brownien et réalité moléculaire". In: *Annales de Chimie et de Physique* 18 (1909), pp. 5–104.

[24] Y. Han et al. "Brownian motion of an ellipsoid". In: *Science* 314 (5799 2006), pp. 626–630.

[25] Ayan Chakrabarty et al. "Brownian motion of arbitrarily shaped particles in two dimensions". In: *Langmuir* 30 (46 2014), pp. 13844–13853.

[26] Ayan Chakrabarty et al. "Effects of translation–rotation coupling on the displacement probability distribution functions of boomerang colloidal particles". In: *Soft Matter* 12 (19 2016), pp. 4318–4323.

[27] Lyndon Koens, Maciej Lisicki and Eric Lauga. "Effects of translation–rotation coupling on the displacement probability distribution functions of boomerang colloidal particles". In: *Soft Matter* 13 (16 2017), pp. 2977–2982.

[28] Daniela Kraft et al. "Brownian motion and the hydrodynamic friction tensor for colloidal particles of complex shape". In: *Physical review E* 88 (5 2013), p. 050301.

[29] Jerome Fung and Vinothan N. Manoharan. "Holographic measurements of anisotropic three-dimensional diffusion of colloidal clusters". In: *Physical review E* 88 (2 2013), p. 020302.

[30] Alexander V. Butenko et al. "Coiled to diffuse: Brownian motion of a helical bacterium". In: *Langmuir* 28 (36 2012), pp. 12941–12947.

[31] Francis Perrin. "Mouvement brownien d'un ellipsoide - I. Dispersion diélectrique pour des molécules ellipsoidales". In: *Journal de Physique et Le Radium* 5.10 (1934), pp. 497–511.

[32] Francis Perrin. "Mouvement Brownien d'un ellipsoide (II). Rotation libre et dépolarisation des fluorescences. Translation et diffusion de molécules ellipsoidales". In: *Journal de Physique et Le Radium* 7.1 (1936), pp. 1–11.